Master
Vellum

FINAL REPORT

RADAR ENHANCEMENT TECHNIQUES

Report No. 0038-C-F

Prepared For:

National Aeronautics and Space Administration
Goddard Space Flight Center
Greenbelt, Maryland

Under:

Contract No. NAS 5-3232

Comsat Research Branch Code 625

CONDUCTRON CORPORATION
343 S. Main Street
Ann Arbor, Michigan

TABLE OF CONTENTS

TABLE OF ILLUSTRATIONS

1. INTRODUCTION

This report describes work performed under contract NAS-5-3232 dealing specifically with techniques of enhancement of the radar cross-section of passive communications sattelites.

The presently deployed Echo I and Echo II satellites are simple and straightforward in concept. As perfectly conducting spheres, they present a radar echo area of πa^2 (where a is the sphere radius) independently of the location of receiver and transmitter; they do not require attitude stabilization, and being inflatable structures, can be, with relative ease, deployed. [The weight, for example, of the Echo II payload is approximately 500 pounds.]

The limitations of the Echo principal are practical in nature. First, small departures of the inflated structure from being a perfect sphere have been shown, theoretically and experimentally to cause variations in the radar cross-section, as a function of viewing angle. References 1, 2, 3, and 4. These variations can cause scintillations in the time history of the radar cross-section values, resulting in possible degradation of communication performance.

Second, the only way to increase the power reflected to the receiver, using the Echo principal, is to increase the radius of the balloon.

It has therefore been the objective of this study to explore techniques whereby the power reflected to the receiver may be increased without increasing the size of the reflector, or, alternatively, the performance of the reflector may be maintained, reducing the size of the reflector.

The question of how this enhancement can be achieved has been actively pursued in recent years. A summary of this research has been reported by J. Kaiser and I. Kay. Reference 5. The effort reported herein consists of

---

Reference 1: Report No. 0038-2-A-F

Reference 2: Report No. 0038-B-F

Reference 3: Report No. 0038-B-S

Reference 4: Report No. 0038-7-F

These reports have been prepared for NASA under contract NAS-5-3232.

Reference 5: Radio Science, Journal of Research, NBS/USNC-URSI, Vol. 68D, No. 4, April 1964, pp. 515-517.

theoretical and experimental investigation of enhancement techniques, some of which have been proposed before, with the objective of exploring in detail their mechanisms, establishing their limitations, and determining avenues for future development.

2. SUMMARY AND ABSTRACT OF THE INVESTIGATION

2.1 Electromagnetic Lenses

Electromagnetic lenses cause the rays to be bent by refractive effects so as to compress the energy reflected from the lens into a narrow angular sector. As this sector is narrowed, the gain increases, and in the limiting case of a focused reflector, the radar cross-section achieves the value $4\pi(\frac{A}{\lambda})^2$, where A is the geometric cross-sectional area, and λ is the wavelength.

The refraction is achieved by utilization of a medium of variable relative (to free space) permittivity. For a spherically symmetric lens, requiring no attitude stabilization, two basic principles can be used; in the Eaton-type lens, entering rays are caused to change their direction solely through the use of refraction; in the Luneberg, or Siegel-Luneberg type, the lens is coated with a partially reflecting surface; rays entering the lens are first refracted and then reflected from the rear surface. The optimal coating introduces a factor of 4/27 into the radar cross-section obtained. If the lens is attitude stabilized, the rear surface can be coated with a perfect conductor.

The analysis of the operation of these lenses is greatly simplified by use of geometric optics. This type of analysis has been carried out in this program, and both the technique of lens synthesis have been established and the gain obtainable for a given bistatic sector has been determined. Experimental measurements on a Siegel-Luneberg lens have been performed. The methods of geometric optics do not take into account the effects of polarization. To illustrate these effects, an analysis of the Eaton lens, using exact electromagnetic theory, was performed.

2.2 Lenticular Segments

A lenticular segment is a spherical "cap." (See Figure 2.2-1)

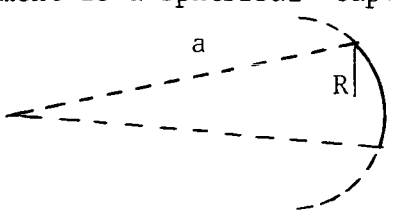

Figure 2.1

Such a cap, of diameter 2R, can be a section of a sphere of radius a, where a >>R. Consequently, the specular radar cross-section of such a cap, πa^2, can be made to be much greater than that of a sphere of radius R. Aside from the obvious need for attitude control of this type of reflector, the principal electromagnetic problem is the effect of the edge. Previous work, done at Conductron, analyzing the effect of this edge, has shown that the field contribution of the edge above is of the same order of magnitude as that of the specular return. Consequently, these two returns have an interference pattern which causes substantial scintillations in the radar cross-section as a function of aspect. An experimental program was carried out to display these scintillations.

2.3 Diffuse Scattering Mechanisms

By placing a large number of discrete scattering centers on the surface of a sphere, many authors have estimated that the radar cross-section can be increased relative to the nominal specular cross-section. An investigation of this effect was pursued to obtain a quantitative description. The example chosen was the use of randomly oriented dipoles placed on a sphere. A formula was obtained which gives the average radar cross-section as a function of dipole density. This formula is analogous to Lambert scattering from a roughened surface.

2.4 Surface Waves

The concept of using a mesh-type spherical surface has been suggested as a means of securing cross-sectional enhancement. This concept has been investigated, using theoretical analysis of a specific wire-mesh balloon structure. The results of experiments performed on flat wire mesh plates resulted in a theory based upon the generation of surface waves on this structure, causing a prediction of radar cross-section enhancement.

3. CONCLUSIONS AND RECOMMENDATIONS

3.1 Electromagnetic Lenses

The electromagnetic lens has the principal advantage that it does not require attitude control. The following table is a listing of the gain available for such a device as a function of the required bistatic coverage.

TABLE 3.1

$\sigma(db > \pi a^2)$	Bistatic Coverage
21.1	10^o
15.2	20^o
11.8	30^o
9.3	40^o
7.5	50^o
6	60^o
4.8	70^o
3.8	80^o
3	90^o

The angle, in degrees, is the maximum angle between the transmitting and receiving directions, and the cross-section is the value that can be achieved for all intermediate angles. As the required bistatic coverage decreases, the limiting case of a focused lens is approached; for a spherically synthetic coated Siegel-Luneberg lens, this cross-section has the limiting value $\sigma/\pi a^2 = \frac{16\pi^2}{27}\left(\frac{a}{\lambda}\right)^2$. The following table gives the gain for a 10 foot radius focused, spherically symetric reflector, and the radius of the sphere of equivalent cross section as a function of frequency.

TABLE 3.2

f(MC)	$\sigma(db > \pi a^2)$	Radius of Equivalent Sphere (ft)
500	15	118
1,000	21	472
2,000	27	1,888
4,000	33	4,552
8,000	39	18,208

It is apparent that for narrow bistatic coverage, the lens has an extremely high gain relative to the sphere. As has been defined above, the bistatic angle is the angle between the receiving and transmitting direction. However, both Tables3.1 and 3.2 are applicable to a more general situation. Suppose that the angle between the receiving direction and the transmitting direction varies between a fixed value, θ_o, and $\theta_o + \theta$. (See Figure 3.1)

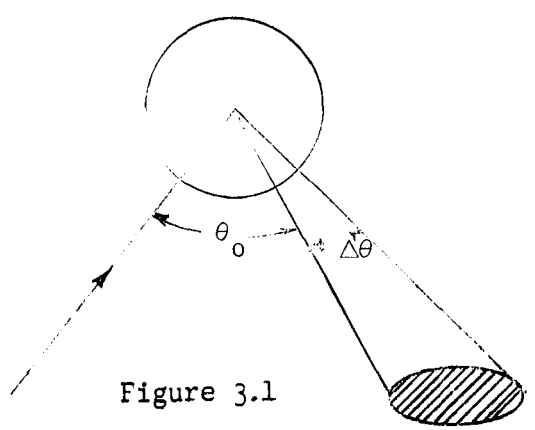

Transmitter

Figure 3.1

Receiver location zone

Then Table 3.1, with θ replacing the bistatic angle, continues to apply, and as $\theta \to 0$, Table 3.2 is applicable. This is particularly applicable to the case in which it is desired to establish jam-proof and non-interceptible communication between two fixed ground stations. For a synchronous satellite such communication could be maintained on a twenty-four hour basis, for a

non-synchronous satellite, the communication would be restricted to those times at which the satellite was in proper position. Using several such non-synchronous satellites, the usable transmission time could be increased.

The only fundamental disadvantage of the spherically symmetric lens is the possible weight penalty. The specific gravity of suitable commercially available dielectric materials is approximately 1/3. Thus the 10 foot radius sphericallens to which Table 3.2 is applicable could weigh as much as 8,000 pounds! A 500 pound lens, comparable in weight to Echo, would have a radius of 1.8 ft; a focused reflector with this diameter would have the same cross-section as Echo II only for frequencies greater than 9,000 MC. Thus its usefulness as a passive link would be limited to X-band, and higher, frequencies.

It is recommended that research be continued to develop light weight refractive media for the construction of dielectric lenses. Logical solutions to this problem are the use of dipole-loaded foams, printed circuits, and wire grids. Perhaps of greater potential for the passive satellite application is the use of artificial dielectrics of three dimensional wire grid. Stanford Research Institute (Reference 6) has used these structures in the design of lens antennas. The principals developed are applicable to the spherical lens. A possible mode of construction is to utilize concentric mylar spheres, on which the grids are imprinted. This construction is well within the state of the art.

3.2 Lenticular Segments

There are two basic problems presented by the use of lenticular segments. The first, and most formidable, is the development of a stabilization system. Methods proposed for this system use either a gravity gradient or inertial orientation sensor. The hard part of the problem is the production of stabilizing forces.

Reference 6: AFCRL 1107, Report 3, AF 19(604)-8059.

The second is the elimination of the effect of the edge on the radar cross-section pattern. This is a problem of combining a suitable shape for electromagnetic purposes with mechanical feasibility.

The basic simplicity, from the electromagnetic point of view, of the lenticular segment make it an attractive device. In this program, the effects of the edge were studied to a sufficient extent to cause us to recommend just the mechanical problems.

3.3 Diffuse Scattering Mechanisms

The problem specifically analysed was that of the enhancement produced by placing, with random orientation, resonant dipoles on the surface of a sphere. This could, in practice, be achieved by either putting non-conducting pieces, or slots, on a conducting sphere, or printing conducting dipoles on a non-conducting sphere. The principal result is that the gain is given by:

$$\frac{\sigma}{\pi a^2} \simeq \frac{3}{2} \cos^2 \beta/2 \left[\frac{5n}{3\pi} \right]^2,$$

where β is the bistatic angle and n is the number of dipoles per $\lambda/2 \times \lambda/2$ area. For $n = 2$, we see that a 2.3 db gain is obtained, and for $n = 3$, a 5.8 db gain. As n increases, the formula becomes less reliable, as its derivation ignores mutual coupling among the dipoles.

The advantages of this technique is that it is achieved with no increase in weight, and perhaps little increase in manufacturing cost.

There are two disadvantages. First, the value of σ obtained is an expected value, and scintillations are expected. Second, the use of resonant dipoles implies a very narrow (about 10%) frequency bandwidth. This frequency bandwidth can be increased by replacing the dipoles by planar spirals, which are known to be broad bandwidth structures.

It is recommended that further study be carried out to increase the bandwidth and the enhancement caused by distributing resonant structures on the

surface of a sphere. It is anticipated that the use of planar broadband structures, such as spirals and log-periodic arrays and other devices can be placed on the surface to achieve optimum enhancement, at no cost in weight.

3.4 Surface Waves

The principal result obtained in this investigation is that for a specific balloon, constructed of wire mesh, the theoretical enhancement ranged from 2 db, at 2,000 MC to 8 db at 6,000 MC. The fundamental mechanism responsible for this effect is the fact that mesh structures, having a non-zero surface impedance, support surface waves, in contrast to perfectly conducting surfaces, which have zero surface impedance. The surface impedance is defined as the ratio between the tangential electric field and the surface currents. A surface wave is energy which propagates along the surface, with a phase velocity determined by the surface properties, and which does not radiate. When the surface wave encounters a discontinuity, such as the termination of a wire mesh panel, currents are generated in this termination which cause radiation. The balloon in question was constructed of a large number of these mesh panels, and the resulting excitation of the edges joining these panels caused the enhancement.

In as much as wire mesh structures are being considered as materials for future passive communication satellites, it is recommended that studies be continued in studying the electromagnetic properties of these structures; the results obtained already indicate that they do not behave as specular reflectors, even for mesh sizes which are much smaller than the wavelength; their enhancement effect is, as in the case of diffuse scatterers, (4-6 db) obtained at no cost in weight; however the frequency dependence of the radar cross-section pattern and the possible scintillations in the pattern warrant further investigation, from the point of view of effect on performance as a communication satellite.

4. RECAPITULATION OF RECOMMENDATIONS

To sum up, there have been evaluated a variety of enhancement mechanisms:

1. The most promising, from the point of view of amount of enhancement which can be obtained, is the dielectric lens. It is felt that it is possible to synthesize light weight lenses, using artificial dielectrics to overcome the principal disadvantage of these structures--their weight.

2. From the point of view of obtaining moderate enhancement (up to 10 db) at no cost in weight, distributing resonant structures on the balloon surface and using the surface wave effects of wire mesh structures are both feasible. It is felt that the principal disadvantage of this effect--sensitivity to frequency--can be overcome by using broadbanding techniques. A second disadvantage is the presence of scintillations.

3. From the point of view of electromagnetic simplicity, the lenticular segment is an attractive device for obtaining enhancement, for a fixed size satellite, comparable to that which can be obtained using lenses; provided that the mechanical problems of deployment and stabilization can be overcome, with elimination of electromagnetic edge effects.

5. TECHNICAL DOCUMENTATION

This section contains the technical documentation of the preceding sections. It consists of memoranda and papers written under this portion of NAS-5-3232, arranged and edited to conform to the arrangement of the preceding sections. For the sake of completeness, some work that has been performed internally, at Conductron, under company sponsorship, has been included and identified.

5.1 Electromagnetic Lenses

R.K. Luneberg, in his monograph "Mathematical Theory of Optics" (1944) gave a method of synthesizing variable index of refraction structures with prescribed scattering cross section properties. The "Luneberg Lens" is an example of such a structure. The operation of this lens can be understood by means of the following argument:

It is well-known that, for normal plane wave incidence, the back-scattering cross-section of a flat plate, with area A, is $4\pi A^2/\lambda^2$. This formula is extremely accurate as long as the smallest linear dimension of the plate is larger than λ. If we think of the phenomenon in terms of geometric optics, all the rays which strike the plate are in phase, and are reflected in phase. See Figure 5.1.

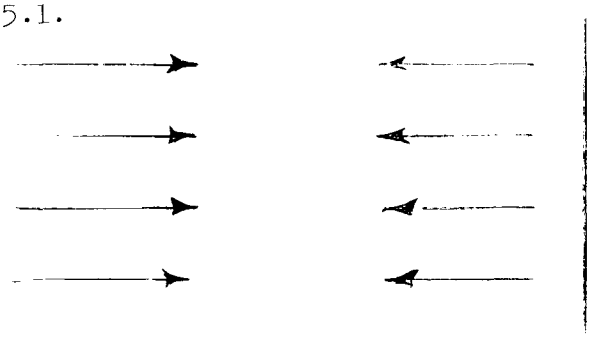

Figure 5.1 Incoming and Reflected Ray Systems for Flat Plate

If the flat plate is replaced by a device which converts the incoming ray system of Figure 5.1 to the reflected ray system of Figure 5.1, the backscattering cross-section of such a device will be the same as that of the flat plate.

The Luneberg Lens is such a device. In Figure 5.2, the ray path for a Luneberg Lens is illustrated.

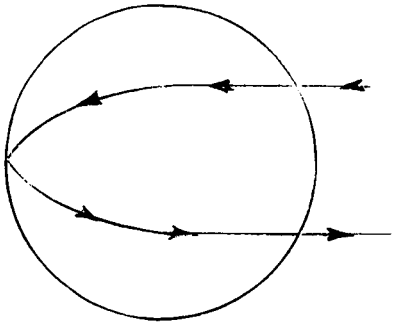

Figure 5.2 Ray Path for Luneberg Lens

The lens is a sphere of radius a made of material whose relative dielectric constant is $\epsilon - \frac{r^2}{a^2}$, where r = radial distance from the center of the sphere. The rear surface is coated with a perfectly conducting material. Each incoming ray is refracted so that the ray system is focused and reflected as indicated in Figure 5.2. Luneberg showed that the above choice of ϵ both guaranteed the correct focusing, but also governed phase in such a fashion as to provide an outgoing ray system equivalent to that in Figure 5.1.

The Luneberg lens, a passive radar cross-section enhancement device is limited inasmuch as the section of the reflector requires that the lens be properly oriented with respect to the illuminating radar. To remove this limitation, K. M. Siegel, introduced the following modification, which is the patented Siegel-Luneberg lens:

If the perfect conductor used as a reflector on the Luneberg lens is replaced by a partially reflecting material which is used to coat the entire sphere, a spherically symmetric reflection system is produced. If the material has reflectivity R, and transmission coefficient T, then the ray paths of Figure 5.2 will be maintained but the return power will be multiplied by a factor T^2R, corresponding to each ray passing through the material twice and being reflected once. If T^2R is maximized, subject to the constraint $T + R = 1$, it is found that $T = \frac{2}{3}$, $R = \frac{1}{3}$, and the product T^2R has the maximum

value 4/27. The Siegel-Luneberg lens therefore has, theoretically, a back-scattering cross-section σ, given by

$$\frac{\sigma}{\pi a^2} = \frac{16\pi}{27} \frac{\pi a^2}{\lambda^2} .$$

Such lenses have been built and tested. In practice, the effect of the dependence of R and T for real materials upon angle of incidence causes a decrease in the gain. Typical measurements for a Siegel-Luneberg lens are described in Conductron Corporation Report No. CAA-1003-1, "Experimental Results of the Siegel-Luneberg Reflector" by Robert R. Graham, July 5, 1961.

The lens described above gives the optimal back-scattering cross-section for a spherically symmetric passive device. It is limited by the fact that it provides extremely narrow angular coverage. For bistatic coverage, de-focusing must be employed. The results described above were first reported by Graham, Siegel, et al ["Optimum Spherically Symmetric Corner Reflectors," URSI Spring Meeting, 1961]; J.E. Eaton [1953], A.F. Kay [1959], and others had previously made major contributions to the practical and theoretical understanding of this subject.

In the remainder of this section, the theoretical basis for the electro-magnetic lens will be developed as a self-contained subject and the capability of such lenses for bistatic passive coverage will be explored. We have also appended several related memoranda.

The starting point, of course, is Maxwell's equations. If in a medium with relative dielectric constant ϵ, relative permeability $\mu = 1$, an electro-magnetic wave with time dependence $e^{-i\omega t}$ is propagated, the electric and magnetic fields, $\underline{E}$ and $\underline{H}$, satisfy the equations

$$\begin{aligned} \nabla \times E - i\omega \underline{H} &= 0 \\ \nabla \times H + i\omega \underline{E} &= 0 \end{aligned} \qquad (5\text{-}1)$$

We shall seek a solution of these equations of the form

$$\underline{E} = e^{i\omega\Phi} \sum_{n=0}^{\sim} \frac{1}{\omega^n} \underline{F}_n. \tag{5-2}$$

The representation (5-2) is known as the Kline-Luneberg expansion; by substituting (5-2) into (5-1), arithmetic manipulation shows that it is necessary that

$$|\nabla\Phi|^2 = \epsilon \tag{5-3}$$

$$\nabla(\nabla\Phi\cdot\underline{F}_{n+1}) - (\nabla\log\epsilon)\cdot\underline{F}_{n+1}\nabla\Phi - \underline{F}_{n+1}\nabla^2\Phi$$

$$-2(\nabla\Phi\cdot\nabla)\underline{F}_{n+1} = i\{\nabla x \nabla x F_n\} \tag{5-4}$$

Equations (5-3) and (5-4) do not, in themselves determine the electromagnetic field. It is known, however, that if complete boundary conditions are given, the solutions to (5-3) and (5-4) are determined, and the series (5-2) is an asymptotic representation of the field. From (5-2) and (5-3) it is seen that the surfaces of constant phase, Φ = constant, satisfy the Hamilton-Jacobi Eiconal Equation,

$$|\nabla\Phi|^2 = N^2, \tag{5-5}$$

where the index of refraction, N, is equal to $\sqrt{\epsilon}$. Thus, for large values of ω, according to geometric optics, the local optical distance is proportional to N, and according to the Hamilton-Jacobi variational principle, the path of a ray between the points P_1 and P_2 is such as to cause the integral

$$\int_{P_1}^{P_2} N ds \tag{5-6}$$

to be a minimum. Suppose that spherical coordinates (n,θ,φ), are introduced that $N = N(r)$ depends only upon r, and $N(r) = 1$ if $r \geq a$. (See Figure 5.3) Then if a ray is incident from the direction $\theta = \pi$, parallel to the z axis, it will

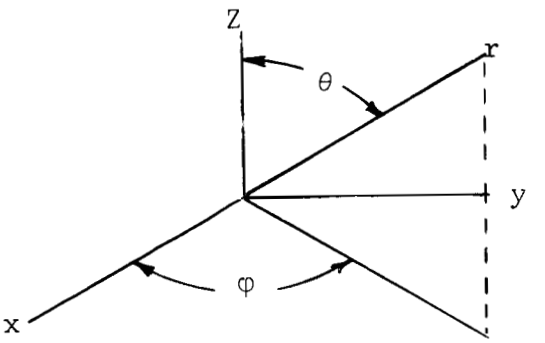

Figure 5.3 Definition of Spherical Coordinates

not deviate from its φ = constant plane, but rather will have a path of the form $\theta = \theta(r)$, and will leave in a direction $\theta = \theta_o$. (See Figure 5.4) The distance b is called the impact parameter.

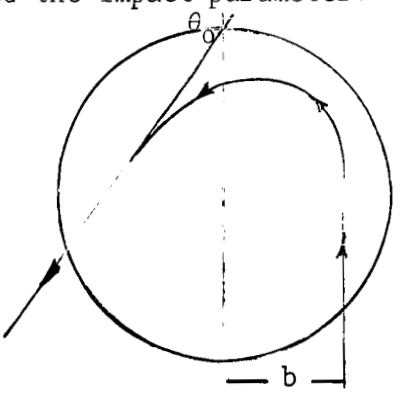

Figure 5.4 Ray Geometry

To determine the function $\theta = \theta(r)$, we make use of the fact that for any two points (r_1,θ_1), (r_2,θ_2) on the ray path, $\theta(r)$ must be such to make the integral (s):

$$\int_{r_1}^{r_2} N(r) \sqrt{1 + r^2 \left(\frac{d\theta}{dr}\right)^2}\, dr$$

a minimum. Applying the calculus of variations to this integral, we obtain:

$$\delta \int_{r_1}^{r_2} N(r) \sqrt{1 + r^2 \left(\frac{d\theta}{dr}\right)^2}\, dr =$$

$$\int_{r_1}^{r_2} \frac{N(r) r^2 \frac{d\theta}{dr}}{\sqrt{1 + r^2 \left(\frac{d\theta}{dr}\right)^2}}\, d(\delta\theta)$$

$$= - \int_{r_1}^{r_2} \delta\theta \; d \left[\frac{N(r) r^2 \frac{d\theta}{dr}}{\sqrt{1 + r^2 \left(\frac{d\theta}{dr}\right)^2}} \right] = 0$$

for all variations, $\delta\theta_r$ which are zero at r_1 and at r_2.

Therefore

$$\frac{r^2 N(r) \frac{d\theta}{dr}}{\sqrt{1 + r^2 \left(\frac{d\theta}{dr}\right)^2}} = \text{constant.} \qquad (5\text{-}7)$$

To determine this constant, we observe that for the incoming ray, $\theta > \frac{\pi}{2}$, $r > a$, and $r \sin\theta = b$.

Thus $N(r) = 1$, $r\cos\theta \frac{d\theta}{dr} + \sin\theta = 0$, and $\frac{d\theta}{dr} = \frac{+ b}{r^2 \sqrt{1 - \frac{b^2}{r^2}}} = \frac{b}{r\sqrt{r^2 - b^2}}$.

Substituting this value of $\frac{d\theta}{dr}$ into (5-7), we find that the constant in (5-7) is precisely b, the impact parameter. From equation (5-8), we then obtain

$$\frac{dr}{d\theta} = \frac{r}{b} \sqrt{r^2 N^2(r) - b^2} \qquad (5\text{-}8)$$

Since $\lim_{n \to 0} r^2 N^2(r) = 0$, from equation (5-8), it is seen that as θ decreases, the value of r will decrease until the smallest value of r, r*, is reached.

This value of r* is determined by the equation

$$r^2N^2(r)/_{r\,=\,r^*} = b^2 \qquad (5\text{-}9)$$

Because of the obvious symmetry; the rest of the ray path is obtained by reflecting the path for $r > r^*$ about the straight line connecting the origin to the point of closest approach. If N(r) is either steadily increasing or steadily decreasing from its value 1 at n = a (as r decreases), the respective values of* will be less than or greater than b. The respective ray paths will then be as in Figures 5.5(a) and 5.5(b).

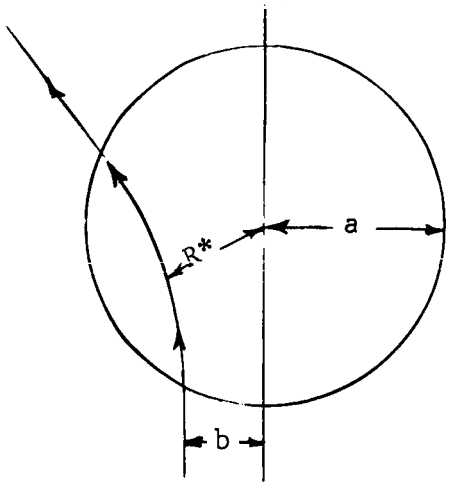

Figure 5.5(a): N(r) < 1

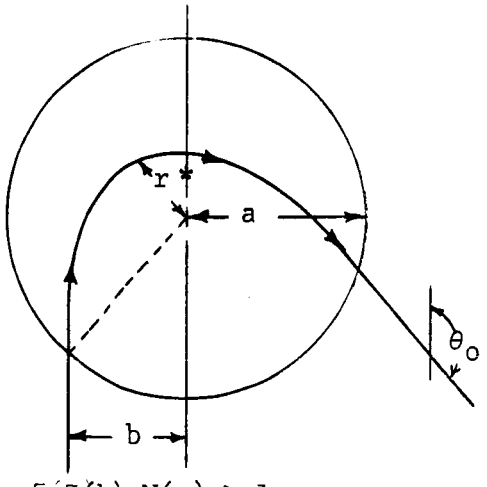

Figure 5.5(b): N(r) > 1

Figure 5.5 Ray Geometry for N(r) < 1 and N(r) > 1

In Figure 5.5 it is assumed that no reflecting material is used to coat the surface of the dielectric.

In Figure 5.5, it is seen that the exit angle, θ_0, is given by

$$\theta_0 = 2 \sin^{-1} \left(\frac{b}{a} \right) + 2b \int_{r^*}^{a} \frac{dr}{r\sqrt{r^2N^2(r) - b^2}} - \pi \qquad (5\text{-}10)$$

The term

$$b \int_{r^*}^{a} \frac{dr}{r\sqrt{r^2N^2(r) - b^2}} = \Phi(b)$$

is seen, from (5-8), to represent the change in θ as the ray enters and reaches its minimum value, r^*. θ_0, of course, depends upon b. From the geometry of Figure 5.5(b), it is apparent that as $b \to 0$, $\theta_0 \to \pi$. It is also apparent that as θ_0 increases, b must decrease.

Now consider the scattered rays contained in the solid angle defined by $\theta_0 < \theta < \theta_0 + \Delta\theta_0$. Since θ_0 (b) is a monotonic function, these rays will come from a circular ring of incoming rays whose impact parameter satisfies

$$b(\theta_0 + \Delta\theta_0) < b < b(\theta_0).$$

The area of this ring is approximately

$$-2\pi b(\theta_0) \frac{db}{d\theta_0}(\theta_0)\, \Delta\theta_0 = -\pi \left[\frac{d}{d\theta_0} b^2(\theta_0) \right] \Delta\theta_0$$

The area on the sphere of radius R in the solid angle is $2\pi R^2 \sin\theta_0 \Delta\theta_0$. Since, in geometric optics, the conservation of energy is expressed in terms of the number of rays passing through a given area, we have the bistatic cross-section $\sigma(\theta_0)$ expressed as

$$\sigma(\theta_0) = \frac{4\pi R^2 \left[-\pi \frac{d}{d\theta_0} b^2(\theta_0) \right] \Delta\theta_0}{2\pi R^2 \sin\theta_0 \Delta\theta},$$

or

$$\frac{d}{d\theta_0} b^2(\theta_0) = -\frac{1}{2\pi} \sigma(\theta_0) \sin\theta_0.$$

Since we have already seen that as $\theta_0 \to \pi$, $b \to 0$, we have

$$2\pi b^2(\theta_0) = \int_{\theta_0}^{\pi} \sigma(\theta')\sin\theta' d\theta' \tag{5-11}$$

which determines the relationship between the impact parameter and the angle at which the ray leaves. If (θ_0) is prescribed, (5-11) determines $b(\theta_0)$. Equation (5-10) then is an integral equation which determines $N(r)$.

Following Luneberg, we shall find an explicit solution for equation (5-10). Let $p(r) = rN(r)$ and $\tau(r) = \log r$. Then when $r = r^*$, $p = b$ and when $r = a$, $P = a$. Therefore,

$$\Phi(b) = b \int_b^a \frac{d\tau}{dp} \frac{1}{\sqrt{p^2 - b^2}} \, dp$$

Let t be a parameter $0 < t < a$, and let us consider

$$\int_t^a \frac{\Psi(b)}{\sqrt{b^2 - t^2}} \, db = \int_t^a \frac{b}{\sqrt{b^2 - t^2}} \int_b^a \frac{d\tau(p)}{\sqrt{p^2 - b^2}} \, db$$

$$= \int_t^a \left\{ \int_t^p \frac{}{\sqrt{b^2 - t^2}\sqrt{p^2 - b^2}} \, db \right\} d\tau(p)$$

$$= \frac{\pi}{2} \tau(p)\Big|_{p=t}^{p=a} .$$

Let $r = r(t)$, $N(r) = N(t)$ be a parametric description of r and $N(r)$. Then:

$$r = a \exp\left[-\frac{2}{\pi} \int_t^a \frac{\Psi(b)db}{\sqrt{b^2 - t^2}} \right]$$

$$N(r) = \frac{t}{a} \exp\left[\frac{2}{\pi} \int_t^a \frac{\Psi(b)db}{\sqrt{b^2 - t^2}} \right] \tag{5-12}$$

Equations (5-11) together with equation (5-10), and

$$\Psi(b) = \frac{1}{2}\ (\pi + \theta_0) - \sin^{-1}\left(\frac{b}{a}\right)$$

$$2\pi b^2(\theta_0) = \int_{\theta_0}^{\pi} \sigma(\theta')\sin\theta' d\theta' \qquad (5\text{-}12a)$$

are adequate to determine N(r) for a prescribed $\sigma(\theta)$, inasmuch as equations (5-10) and (5-11) determine Φ (b) as a function of b, by elimination of θ_0.

In order to see how equations (5-12) and (5-12a) can be used to synthesize a lens with a prescribed bistatic cross section, let us seek to construct a lens for which

$$\begin{aligned} \sigma(\theta) &= B\pi a^2 && \beta < \theta < \pi \\ &= 0 && 0 < \theta < \pi \end{aligned} \qquad (5\text{-}13)$$

Such a lens would give uniform gain over an isotropic reflector for bistatic angles up to $\pi - \beta$. From the last equation of the set (5-12), and (5-12a), we find that

$$\begin{aligned} b^2(\theta_0) &= a^2 b \cos^2\frac{\theta_0}{2} && \beta < \theta_0 < \pi \\ &= a^2 G \cos^2\beta/2 && 0 < \theta_0 < \beta \end{aligned} \qquad (5\text{-}14)$$

From equation (5-14) we see that, since $b^2(\theta_0) \leq a^2$ for all θ_0, G has the maximum value

$$G_{max} = \frac{1}{\cos^2\beta/2} \qquad (5\text{-}15)$$

TABLE 5.1

Maximum Uniform Gain vs. Bistatic Coverage

G_{max} (db > πa^2)	Bistatic Angle ($\pi - \beta$)
21.1	10^o
15.2	20^o
11.8	30^o
9.3	40^o
7.5	50^o
6.0	60^o
4.8	70^o
3.8	80^o
3.0	90^o

Using $G = G_{max}$, we find then from (5.12a) that

$$\Psi(b) = \frac{\pi}{2} + \cos^{-1}\left(\frac{b}{a}\cos\beta/2\right) - \sin^{-1}\left(\frac{b}{a}\right)$$

$$= \cos^{-1}\left(\frac{b}{a}\cos\beta/2\right) + \cos^{-1}\left(\frac{b}{a}\right)$$

Putting this value of $\Phi(b)$ into (5-12), r and N(r) are determined as functions of the parameter t. Now,

$$\int_t^a \frac{\cos^{-1}\frac{b}{a}}{\sqrt{b^2 - t^2}}\,db = \int_t^a \frac{b}{\sqrt{b^2 - t^2}} \int_b^a \frac{d\xi}{\xi\sqrt{\xi^2 - b^2}}\,db$$

$$= \int_t^a \left(\int_t^\xi \frac{bdb}{\sqrt{b^2 - t^2}\sqrt{\xi^2 - b^2}} \right) \frac{d\xi}{\xi} = \frac{\pi}{2}\log\frac{a}{t}\,.$$

Therefore

$$\frac{2}{\pi}\int_t^a \frac{\psi(b)}{\sqrt{b^2 - t^2}}\,db = \log\frac{a}{t} + \frac{2}{\pi}\int_t^a \frac{\cos^{-1}\left(\frac{b}{a}\cos\beta/2\right)}{\sqrt{b^2 - t^2}}\,db$$

Thus, the parametric representations (5-12) become:

$$r = t\exp\left[-\frac{2}{\pi}\int_t^a \frac{\cos^{-1}\left(\frac{b}{a}\cos\beta/2\right)}{\sqrt{b^2 - t^2}}\,db\right]$$

$$N(r) = \exp\left[\frac{2}{\pi}\int_t^a \frac{\cos^{-1}\left(\frac{b}{a}\cos\beta/2\right)}{\sqrt{b^2 - t^2}}\,db\right] \qquad (5\text{-}16)$$

To estimate the integrals in (5-16), we write

$$\frac{2}{\pi}\int_t^a \frac{\cos^{-1}\left(\frac{b}{a}\cos\beta/2\right)}{\sqrt{b^2 - t^2}}\,db = \frac{1}{\pi}\int_t^a \cos^{-1}\left(\frac{2b^2}{a^2}\cos^2\beta\{2 - 1\}\right) d\log\left[b+\sqrt{b^2 - t^2}\right]$$

$$= \frac{\beta}{\pi}\log\left(a + \sqrt{a^2 - t^2}\right) - \frac{1}{\pi}\cos^{-1}\left(\frac{2t^2}{a^2}\cos^2\frac{\beta}{2} - 1\right)\log t$$

$$+ \frac{2}{\pi}\int_t^a \frac{1}{\sqrt{a^2\sec^2\beta\{2 - b^2}}\log\left[b + \sqrt{b^2 - t^2}\right]\,db$$

Therefore, for small values of t,

$$r \sim t^2 C$$

$$N(n) = 1/Ct, \text{ where}$$

$$C = (2a)^{-\beta/\pi}\exp\left[-\frac{2}{\pi}\int_0^a \frac{\log 2b\,db}{\sqrt{a^2\sec^2\beta/2 - b^2}}\right]$$

Thus $N(r) \sim \frac{1}{\sqrt{Gr}}$, as $r \to 0$. Hence, for a generalized Eaton lens to give uniform bistatic coverage it is necessary that the dielectric constant have a singularity of the form 1/r as r→0. Consequently, in the practical construction of such a lens the correct value of N(r) can only be approximated. If the value of N(r) is correct except for small central sphere of radius a*, only rays whose minimal distance, r*, is less than a*. Now, for the relationship (5-9), the corresponding impact parameters, b, satisfy

$$b^2 = (r^*)^2 N^2(r^*) \sim r^*/C \leq a^*/C.$$

Therefore, the error in the cross-section $\leq \frac{a^*}{C'a^2}$.

An alternative to a generalized Eaton lens is the generalized Luneberg lens, in which a reflector is used, and the ray path is as in Figure 5.6.

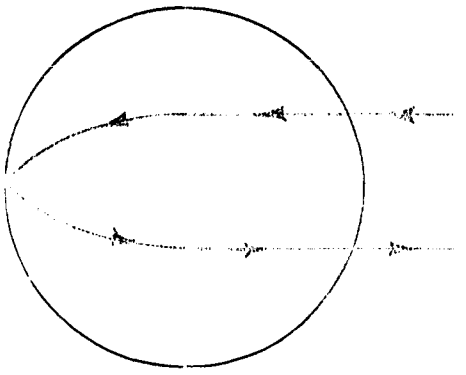

Figure 5.6 Generalized Luneberg Reflector

For this configuration, equations (5-12) and (5-12a) are unchanged, except for the first equation in (5-12a), which becomes:

$$2\Psi(b) = \frac{1}{2}(\pi + \theta_0) - \sin^{-1}\left(\frac{b}{a}\right).$$

For the ideal bistatic coverage, defined by (5-14) and (5-15), the preceding computations still apply, except that

$$\frac{2}{\pi}\int_t^a \frac{\Psi(b)}{\sqrt{b^2 - t^2}}\,dt \sim \frac{1}{2}\log\frac{a}{t} + \frac{1}{\pi}\int_t^a \frac{\cos^{-1}\left(\frac{b}{a}\cos\beta/2\right)}{\sqrt{b^2 - t^2}}\,,$$

which for small t, becomes

$$\frac{\beta}{2\pi}\log 2a + \frac{1}{\pi}\int_0^a \frac{1}{\sqrt{a^2\sec^2\beta/2 - b^2}}\log 2b\,db + \log\frac{a}{t}$$

In this case,

$$r \sim C't$$

$$N(r) \sim 1/C'.$$

Thus, N(r) is bounded, so that there is no theoretical reason that the correct value of N(r) could not be achieved. However, if the lens is not stabilized, a Siegel-Luneberg coating must be used, which reduces the gains given in Table 5.1, for small angles, by approximately 8 db.

If, for this configuration,

$$N^2(r) = 1 + 2\left[1 - \left(\frac{r}{a}\right)^2\right],$$

it is easy to find:

$$\sigma(\theta_0) = \frac{\pi a^2 (1-\alpha)^2}{\left[(1+\alpha)^2\cos^2\frac{\theta_0}{2} + (1-\alpha)^2\sin^2\frac{\theta_0}{2}\right]^2}$$

which has a gain of $\frac{1}{(1-\alpha)^2}$ at $\theta_0 = \pi$ (back-scattering) and a half power point:

$$\theta_0 = 2\tan^{-1}\left[\frac{1+\alpha}{1-\alpha}\,\frac{1}{\sqrt{\sqrt{2}-1}}\right]$$

The above discussion has been in terms of geometric optics. For the

original Luneberg lens, the geometric optics successfully describes the ray paths. However, calculation of $\Phi(b)$ and evaluation of θ_0 from (5-10), gives: $\theta_0 = \pi$ for all b, so that (5-11) is inapplicable to determine the back-scattering, and other arguments must be applied. The intuitive arguments given at the beginning of this section do, in fact, give the correct answer. However, for the focused Eaton lens, where $N^2(r) = \frac{2a-r}{r}$, again $\theta_0 = \pi$ for all b. However, because there is no reflection, but only refraction, for back-scattering, the effect of polarization gives zero cross-section. The following discussion is a discussion of this phenomenon, taking polarization into account:

Scattering from the Eaton Lens

The Eaton lens is a particular example of the class of Luneberg lenses. The general Luneberg lens is a dielectric sphere in which the index of refraction is a function of the radius only. For the Eaton lens in free space, the index of refraction is given by

$$n^2 = \frac{2a - r}{r} ,$$

where a is the radius of the outer surface, and a geometric optics analysis based on Fermat's principle shows that each ray of an incident plane electromagnetic wave suffers a 180^o change in direction as it passes through such a lens. The spherical symmetry requires the ray to describe a symmetrical path in a plane passing through the sphere axis which is parallel to the original ray direction. See Reference 7. (See Figure 5.7)

Since the intensity and phase of the incident plane wave are uniform over the polar plane, the intensity and phase of the refracted wave are uniform over the same plane, but the effect of the lens on the direction of polarization of each incident ray is to generate a refracted wave for which the polarization direction is a function of position on the polar plane of the lens.

Figure 5.7 shows the lens and the system of co-ordinates which will be adopted. The incident plane wave is assumed to be propagating in the negative z direction and polarized in the y direction. If, for each ray, we resolve the electric field vector of the incident wave along the radial and polar angle directions, we find that the radial component is reversed in direction by the lens action but the polar angle component is unchanged. Thus, in the region of the polar plane the refracted wave is given by

$$\bar{E}(\bar{\rho}) = E \left(- \hat{x} \sin 2\phi + \hat{y} \cos 2\phi \right) e^{ik(z+\alpha)} \quad |\rho| < a \qquad (5\text{-}17)$$

Reference 7: Huynen, J. R.: "Theory and Design of a Class of Luneberg Lenses", 1958 I.R.E. WESCON Convention Record, Pt. 1, pp. 219-230.

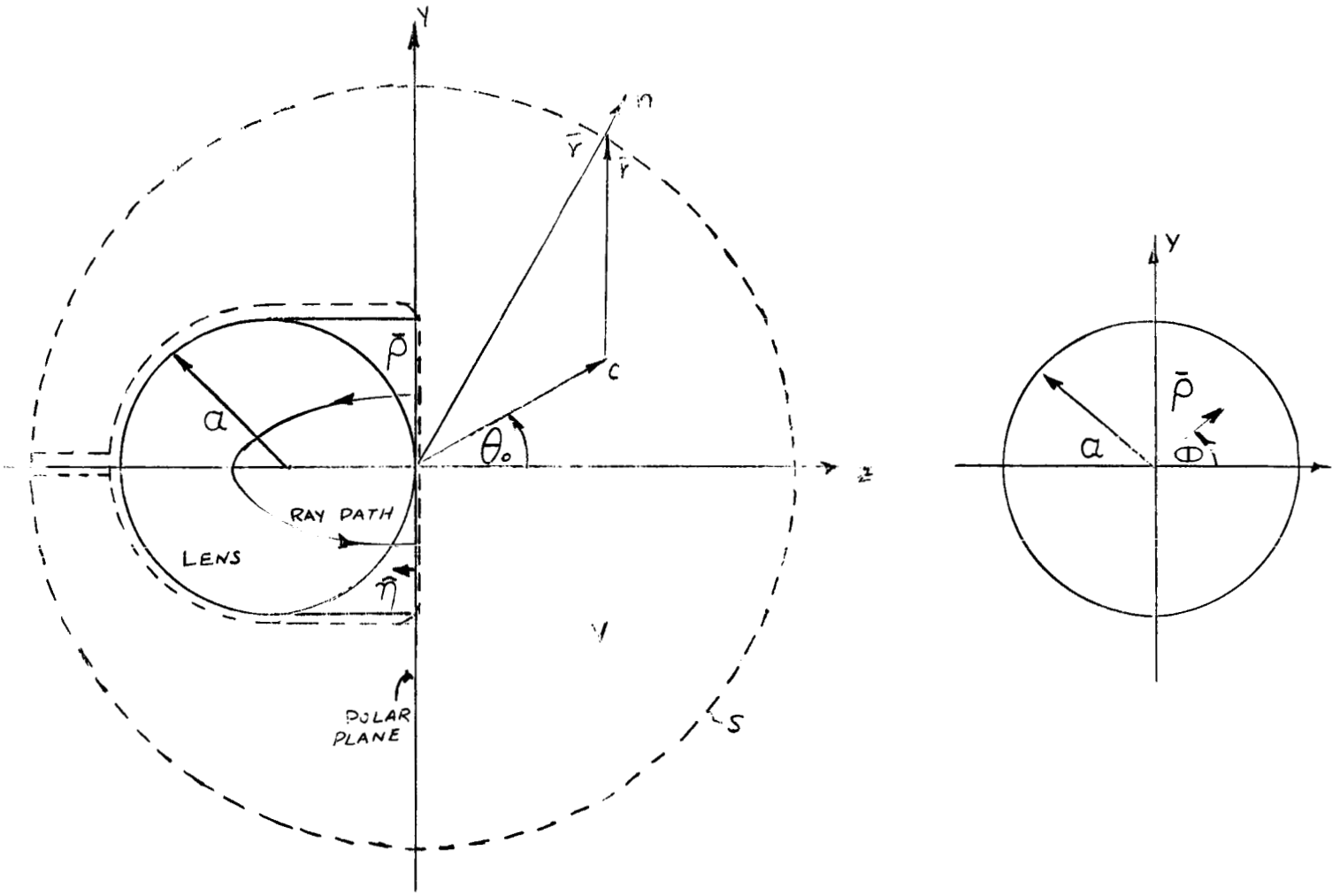

Figure 5.7 Ray Path in an Eaton Lens

where α is an arbitrary phase constant depending on the electrical path length through the lens and the particular time origin chosen.

If the wavelength of the incident wave is zero, eq. (5-17) is exact. If the wavelength is small compared with the radius of the lens, the equation is approximately correct, and we may use it to evaluate the scattered field.

Now for each cartesian component of the electric field vector of the refracted wave the free space wave equation is

$$\nabla^2 E_\alpha (\bar{r}) + k^2 E_\alpha (\bar{r}) = 0 \qquad (5\text{-}18)$$

and the corresponding free space Green's function is defined by

$$\nabla^2 G (\bar{r}, \bar{R}) + k^2 G(\bar{r}, \bar{R}) = -\delta (\bar{r} - \bar{R}), \qquad (5\text{-}19)$$

for which the solution, neglecting the advanced potential terms is

$$G (\bar{r}, \bar{R}) = \frac{1}{4\pi} \frac{e^{ik |\bar{r}-\bar{R}|}}{\bar{r} - \bar{R}} \qquad (5\text{-}20)$$

We apply Green's theorem to the spherical volume of radius r but excluding the lens and its projection on the polar plane, as shown by the broken contour in Figure 5.7 . Then

$$\int (G\nabla^2 E_\alpha - E_\alpha \nabla^2 G)\, dv = (G\nabla E_\alpha - E_\alpha \nabla G)\cdot d\bar{S},$$

where $d\bar{S}$ is directed away from the interior.

Substituting eq. (5-18), we obtain directly

$$\int - E_\alpha (\nabla^2 G + k^2 G)\, dv = \int (G\nabla E_\alpha - E_\alpha \nabla G) \cdot d\bar{S},$$

which, from eq. (5-19) and the property of the delta function, reduces to

$$E_\alpha(\bar{R}) = \iint \left\{ G(\bar{r}, \bar{R}) \frac{\partial E_\alpha(\bar{r})}{\partial n} - E_\alpha(\bar{r})\, n \cdot \nabla G(\bar{r}, \bar{R}) \right\} dS(\bar{r}) \tag{5-21}$$

where $\hat{n}$ is the outer normal and the divergence operates on the $\bar{r}$ co-ordinates, i.e.

$$G = \hat{r}' \left(ik - \frac{1}{r'}\right) \frac{e^{ikr'}}{r'}$$

where $\hat{r}'$ is a unit vector in the direction of $\bar{r}'$ in Figure 5.7 . Now $\bar{r}' = \bar{r} - \bar{R}$, and so eq. (5-21) becomes

$$E_\alpha(\bar{R}) = \frac{1}{4\pi} \iint \frac{e^{ik|\bar{r}-\bar{R}|}}{\bar{r} - \bar{R}} \left\{ \frac{\partial E_\alpha(\bar{r})}{\partial n} - E_\alpha(\bar{r})\, \hat{n} \cdot \left(\frac{\bar{r} - \bar{R}}{|\bar{r} - \bar{R}|} \right) ik - \left(\frac{1}{|\bar{r} - \bar{R}|} \right) \right\} dS(\bar{r}). \tag{5-22}$$

If the radius of the spherical surface is made arbitrarily large, its contribution to the integral vanishes, since for arbitrarily large r,

$E_\alpha(\bar{r}) \to F(\phi, \theta) \frac{e^{ikr}}{r}$ and $\bar{r} - \bar{R} \to \bar{r}$, and on the surface $\frac{\partial E_\alpha(\bar{r})}{\partial n} = \frac{\partial E_\alpha(\bar{r})}{\partial r}$.

The integrand vanishes when these substitutions are made.

Over the inner surface only that part coinciding with the polar plane contributes, since the remainder lies in regions of zero field strength if it is placed just outside the lens surface. If we restrict our attention to the determination of the scattered field in the far zone, $\bar{r} = \bar{\rho}$ at $z = 0$ and $|\bar{\rho}| << |\bar{R}|$. Thus, substituting in eq. (5- 22) and discarding the vanishingly small term in $\frac{1}{R^2}$ we obtain for the far zone

$$\bar{E}(\bar{R}) = \frac{e^{ikR}}{4\pi R} \iint \left\{ \frac{\partial \bar{E}(\bar{\rho})}{\partial n} + ikn \cdot R\, \bar{E}(\bar{\rho}) \right\} e^{-ik\bar{\rho}\cdot\hat{R}} dS(\bar{\rho}) \tag{5-23}$$

where $\hat{R}$ is a unit vector in the direction of $\bar{R}$, the three scalar equations represented by eq. (5-22) have been combined as a vector equation, and the surface of integration is the xy plane within the circle $|\bar{\rho}| \leq a$.

We denote the co-ordinates of $\bar{R}$ as (R, ϕ_o, θ_o) and of $\bar{\rho}$ as $(\rho, \phi, \frac{\pi}{2})$, then

$$\hat{R} = \hat{x} \sin\theta_o \cos\phi_o + \hat{y} \sin\theta_o \sin\phi_o + \hat{z} \cos\theta_o$$

$$\bar{\rho} = \hat{x}\rho \cos\phi + \hat{y}\, \rho \sin\phi$$

$$\hat{n} = -\hat{z}$$

$$dS(\bar{\rho}) = \rho\, d\rho\, d\phi$$

and $\bar{E}(\bar{\rho})$ is given by equation (5-18).

Substituting in eq. (5-23) and collecting terms, we obtain

$$\bar{E}(\bar{R}) = -\frac{ikE_{in}(1 + \cos\theta_o)}{4\pi R} \int_0^a \int_{\psi}^{\psi+2\pi} (-\hat{x} \sin 2\phi + \hat{y} \cos 2\phi)\, e^{-ik\rho \sin\theta_o \cos(\phi-\phi_o)}\, d\phi\rho\, d\rho,$$

where the constant exponents, being of no interest, have been omitted.

The substitution $\phi = \alpha + \phi_o$ leads to a restatement of this equation as

$$\bar{E}(\bar{R}) = -\frac{ikE_{in}(1 + \cos\theta_o)}{4\pi R} \int_0^a d\rho\rho \int_{-\pi}^{\pi} \left\{ -\hat{x} \sin(2\alpha + 2\phi_o) + \hat{y} \cos(2\alpha+2\phi_o) \right\} \left\{ \cos(A \cos\alpha) - i \sin(A \cos\alpha) \right\} d\alpha$$

where $A = k\rho \sin\theta_o$.

The inner integrand may be expanded as

$$(\hat{x}\cos 2\phi_o + \hat{y}\sin 2\phi_o)\left\{i\sin 2\alpha \sin(A\cos\alpha) - \sin 2\alpha\cos(A\cos\alpha)\right\} +$$

$$+ (-\hat{x}\sin 2\phi_o + \hat{y}\cos 2\phi_o)\left\{\cos 2\alpha\cos(A\cos\alpha) - i\cos 2\alpha\sin(A\cos\alpha)\right\}.$$

Now $\sin 2\alpha \sin(A\cos\alpha)$ and $\sin 2\alpha\cos(A\cos\alpha)$ are both odd functions of α and vanish on integration, $\cos 2\alpha \sin(A\cos\alpha)$ is odd about $\pm\frac{\pi}{2}$ and so it, too, vanishes, and $\cos 2\alpha\cos(A\cos\alpha)$ is even about both the origin and $\pm\frac{\pi}{2}$ and so the limits may be contracted. Thus we obtain

$$\bar{E}(\bar{R}) = -\frac{ikE_{in}(1 \pm \cos\theta_o)}{4\pi R}\int_0^a d\rho\rho\, 4(-\hat{x}\sin 2\phi_o + \hat{y}\cos 2\phi_o)\int_0^{\frac{\pi}{2}}\cos 2\alpha\cos(A\cos\alpha)\,d\alpha.$$

But $\int_0^{\frac{\pi}{2}}\cos 2\alpha\cos(A\cos\alpha)\,d\alpha = -\frac{\pi}{2}J_2(A)$,

$$\therefore\ \bar{E}(\bar{R}) = \frac{ikE_{in}(1+\cos\theta_o)}{2R}(-\hat{x}\sin 2\phi_o + \hat{y}\cos 2\phi_o)\int_0^a \rho J_2(k\rho\sin\theta_o)\,d\rho.$$

$$\therefore\ |\bar{E}(\bar{R})| = E_{in}\frac{k(1+\cos\theta_o)}{2R}\int_0^a \rho J_2(k\rho\sin\theta_o)\,d\rho$$

$$\text{or}\ |\bar{E}(\bar{R})| = E_{in}\frac{k(1+\cos\theta_o)}{2R}\left[-\frac{2J_o(ka\sin\theta_o)}{k^2\sin^2\theta_o} - \frac{aJ_1(ka\sin\theta_o)}{k\sin\theta_o} + \frac{2}{k^2\sin^2\theta_o}\right]$$

Substituting $k = \frac{2\pi}{\lambda}$, where λ is the wavelength, we obtain finally for the modulus of the scattered electric field strength in the far zone when $\lambda << a$.

$$E = E_{in} \frac{a\,(1 + \cos\theta_o)}{2\pi \frac{a}{\lambda} R \sin^2\theta_o} \left\{ 1 - J_o(2\pi \frac{2}{\lambda} \sin\theta_o) - \pi \frac{a}{\lambda} \sin\theta_o J_1(2\pi \frac{a}{\lambda} \sin\theta_o) \right\} .$$

(5- 24)

Now the differential scattering cross section is defined as the power scattered per unit solid angle per unit incident power density. In the far zone the scattered power flux is $1/2\sqrt{\frac{\epsilon_o}{\mu_o}}\, E^2$ watts/metre^2, but at a radius of R, one square metre subtends at the origin a solid angle of $\frac{1}{R^2}$ steradians, and the incident power flux is $1/2\sqrt{\frac{\epsilon_o}{\mu_o}}\, E_{in}^{\ 2}$ watts/metre^2.

Thus the differential scattering cross section, σ, is given by

$$\sigma = \frac{E^2}{E_{in}^{\ 2}} R^2 \quad \text{metre}^2/\text{steradian}.$$

Hence, from eq. (5-24),

$$\frac{\sigma}{a^2} = \left\{ \frac{1 + \cos\theta_o}{\sin\theta_o} \quad \frac{1 - J_o(2\pi\frac{a}{\lambda} \sin\theta_o) - \pi \frac{a}{\lambda} \sin\theta_o J_1(2\pi\frac{a}{\lambda} \sin\theta_o)}{2\pi\frac{a}{\lambda} \sin\theta_o} \right\}^2$$

This expression is valid only for $a >> \lambda$ and so for the purposes of evaluation it is necessary to have also a large argument approximation for the Bessel functions to be used when $2\pi\frac{a}{\lambda} \sin\theta_o$ is outside the range of the usual tables. Thus for x large

$$J_\rho(x) \approx \frac{\cos\left| s - (\rho + \frac{1}{2})\frac{\pi}{2} \right|}{(\frac{\pi x}{2}.)^{\frac{1}{2}}}$$

On substituting this in the above expression we obtain, after some preliminary trigonometric manipulation,

$$\sqrt{\frac{\sigma}{a^2}} = \frac{1 + \cos\theta_o}{2\pi\frac{a}{\lambda}\sin^2\theta_o} \left| 1 - \left(\frac{a}{\lambda}\sin\theta_o\right)^{\frac{1}{2}} \left\{1 + \frac{1}{\left(\pi\frac{a}{\lambda}\sin\theta_o\right)^2}\right\}^{\frac{1}{2}} \sin\left\{\left(2\frac{a}{\lambda}\sin\theta_o - \frac{1}{4}\right.\right.\right.$$

$$\left.\left.\left. + \frac{1}{\pi}\tan^{-1}\frac{1}{\pi\sin\theta_o}\right)\pi\right\}\right|$$

$J_o(x)$ and $J_1(x)$ are tabulated in Jahnke and Emde for $0 \leq x \leq 15.5$, hence if tables are used for $2\pi\frac{a}{\lambda}\sin\theta_o < 15.5$ and the approximate expression for $2\pi\frac{a}{\lambda}\sin\theta_o > 15.5$, we have, without significant loss of accuracy,

$$\tan^{-1}\frac{1}{\pi\frac{a}{\lambda}\sin\theta_o} \approx \frac{1}{\pi\frac{a}{\lambda}\sin\theta_o}$$

$$\text{and } 1 + \frac{1}{\left(\pi\frac{a}{\lambda}\sin\theta_o\right)^2} \approx 1$$

Thus we have finally the following two expressions for the differential scattering cross section: -

$$\frac{\sigma}{a^2} = \left\{\frac{1 + \cos\theta_o}{\sin\theta_o} \quad \frac{1 - J_o\left(2\pi\frac{a}{\lambda}\sin\theta_o\right) - \pi\frac{a}{\lambda}\sin\theta_o J_1\left(2\pi\frac{a}{\lambda}\sin\theta_o\right)}{2\pi\frac{a}{\lambda}\sin\theta_o}\right\}^2$$

and, to be used when $2\pi\frac{a}{\lambda}\sin\theta_o$ is large,

$$\frac{\sigma}{a^2} = \left\{\frac{1 + \cos\theta_o}{\sin\theta_o} \quad \frac{1 - \left(\frac{a}{\lambda}\sin\theta_o\right)^{\frac{1}{2}} \sin\left|\left(2\frac{a}{\lambda}\sin\theta_o + \frac{1}{\pi^2\frac{a}{\lambda}\sin\theta_o}\right)\right|}{2\pi\frac{a}{\lambda}\sin\theta_o}\right\}^2$$

Since the lens behavior for very small θ_o is of interest, a series in ascending powers of θ_o is useful. By expressing the Bessel functions as power series, replacing $\sin\theta_o$ by θ_o and $\cos\theta_o$ by unity we obtain

$$\frac{\sigma}{a^2} = \frac{1}{16}\pi^6\left(\frac{a}{\lambda}\right)^6\theta_o^4\left(1 - \frac{4}{9}\pi^2\left(\frac{a}{\lambda}\right)^2\theta_o^2 + \ldots\right),$$

(θ_o in radians).

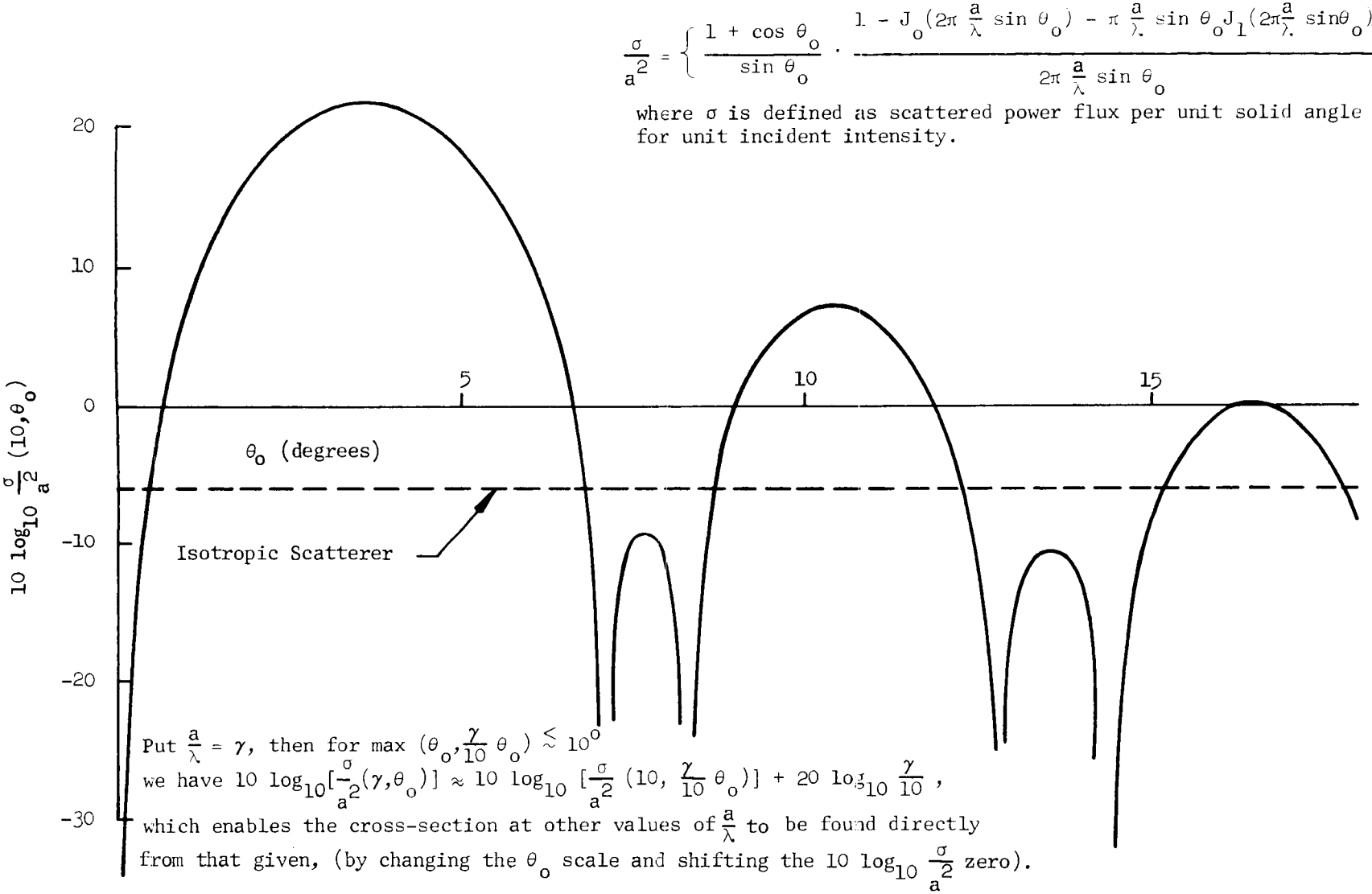

Figure 5.8 Differential Scattering Cross-Section of Eaton Lens

EXPERIMENTAL RESULTS OF THE SIEGEL LUNEBERG REFLECTOR

Introduction

This report describes an experiment performed in the X-band frequency region to determine the radar cross section of a $6\frac{1}{2}$" diameter Siegel Luneberg Reflector. The measured data is presented and compared with theoretical calculations.

Theory

The Siegel Luneberg Reflector was invented by Professor K. M. Siegel and is described in patent application No. 26075. This reflector is unique in that its radar cross section is isotropic in the sense that it is constant and independent of the incidence angle of the incoming waves. In radar applications it is convenient to think of this item as an isotropic corner reflector. It can be used in place of normal corner reflectors or clusters of these with the advantage that the cross section is truly isotropic.

Physically the Siegel Luneberg Reflector is spherical. The reflector is composed of a standard Luneberg lens which has been covered with a special material. In theory the maximum cross section attainable for this reflector is about 8.3 db below a flat plate whose area is equal to the projected geometric area of the spherical reflector. In practice the cross section will be somewhat lower than this because of:

1) Dielectric losses in the Luneberg lens.
2) Variations in the dielectric material that cause defocusing.
3) Losses in the outer covering.

Manufacturer's data for the Luneberg lens show that for items 1 and 2 above, we may expect a loss on the order of 2 db. Our own previous bench measurements indicate that the loss in the outer covering is about 1 db. Taking these losses into consideration, we predict the cross section of the Siegel Luneberg reflector to be 11.5 db below that of an equivalent flat plate.

There is one further loss that at present is unknown. This loss results from not locating the outer covering at the exact focal loci of the central

lens. The focal loci of the particular lens used was found to be about 0.25 inches outside the lens surface. The technique used to attain this spacing was not the best but was used for the sake of expediency. This reflector is the first model that has been constructed. In future models we plan to use a better technique and eliminate this loss.

Measurements

The cross section measurements were made in the anechoic chamber of The University of Michigan Radiation Laboratory. A sketch of the equipment layout is shown in Figure 5.8 . The cross section was determined by comparing the signal backscattered from the reflector under test with the signal received when the reflector was replaced with a conducting sphere of equal diameter. The radar cross section is directly proportional to the amount of power received as may be seen in the standard radar equation:

$$P_R = \frac{P_T \; G_T^2 \; \lambda^2}{(4\pi)^3 \; R^4} \; \sigma$$

G_T = Antenna Gain

P_T = Power transmitted

R = Range

λ = Wavelength

P_R = Power received

σ = Radar cross section

When substituting a sphere for the reflector in the experiment and holding all other parameters constant, the following equation results:

$$\frac{P_R}{P_S} = \frac{\sigma R}{\sigma S}$$

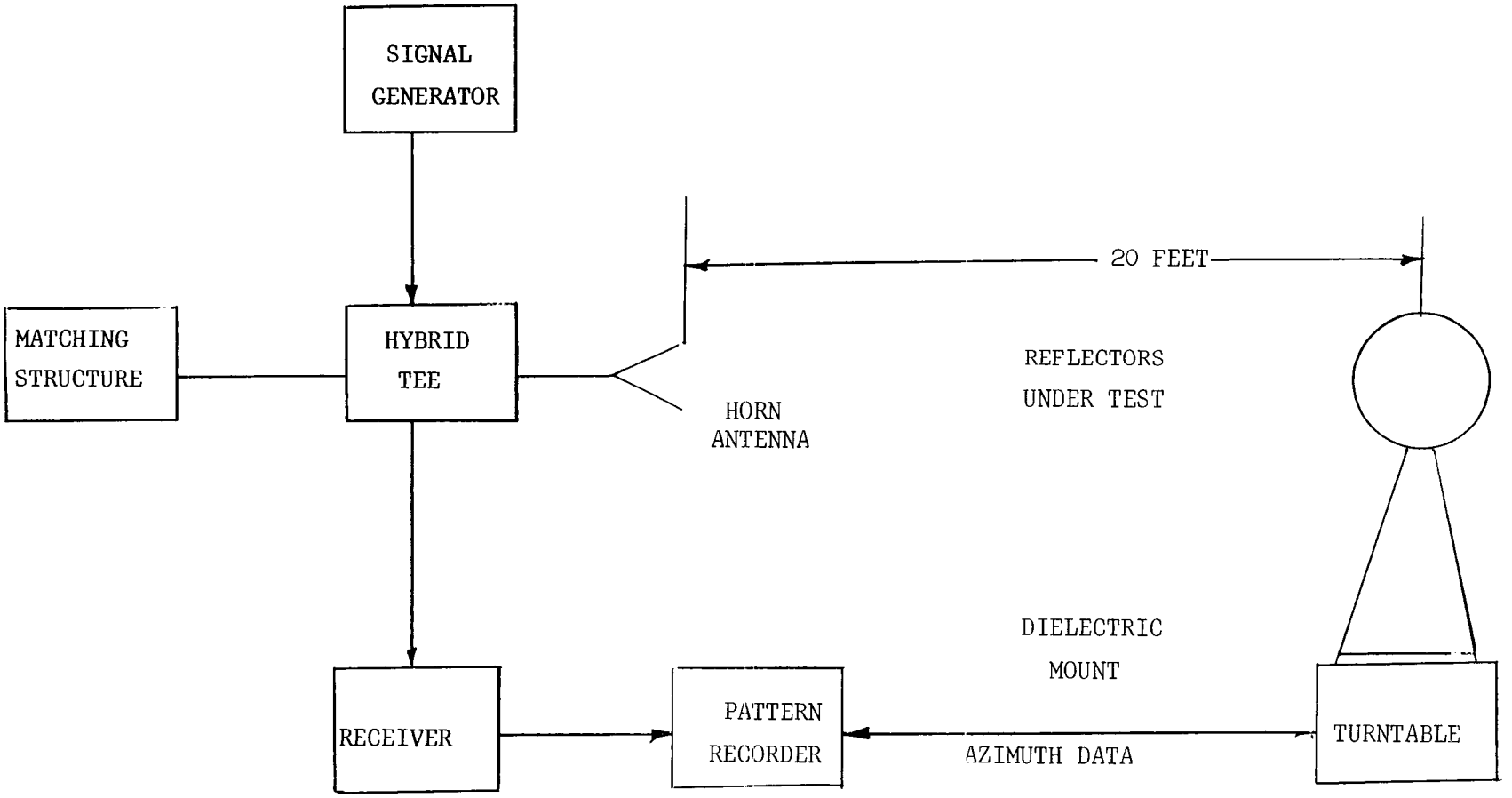

Figure 5.9 Block Diagram of Measurement System

Measurements were made from 8.5 to 10.0 Kmc in increments of 500 mc. At each frequency, measurements were taken for both the reflector and the sphere. Each of these was rotated in azimuth through 360^{o} and the received backscattered signal plotted as a function of angle. The data obtained is shown in figures 5.9, 10, 11, 12. The spacing between the transmitting antenna and the reflectors was 20 feet in all cases so as to achieve far zone conditions.

Discussion

If the cross section of the Siegel Luneberg reflector is 11.5 db below that of an equivalent flat plate, it can be shown that the ratio of the $6\frac{1}{2}$ inch reflector to a $6\frac{1}{2}$ inch conducting sphere is:

$$\frac{\sigma_R}{\sigma_S} = \frac{1}{14.1} \frac{4\pi A}{\lambda_2} \frac{190}{\lambda_2}$$

where λ is in centimeters. Using this equation, the ratio $\frac{\sigma_R}{\sigma_S}$ was calculated at each frequency and compared in Table with average experimental values obtained from the rad data.

TABLE 5.2

Frequency	σ_R/σ_S	
(mc)	Calculated	Measured
8500	11.9 db	11.9 db
9000	12.4 db	11.9 db
9500	12.8 db	11.0 db
10,000	13.3 db	13.4 db

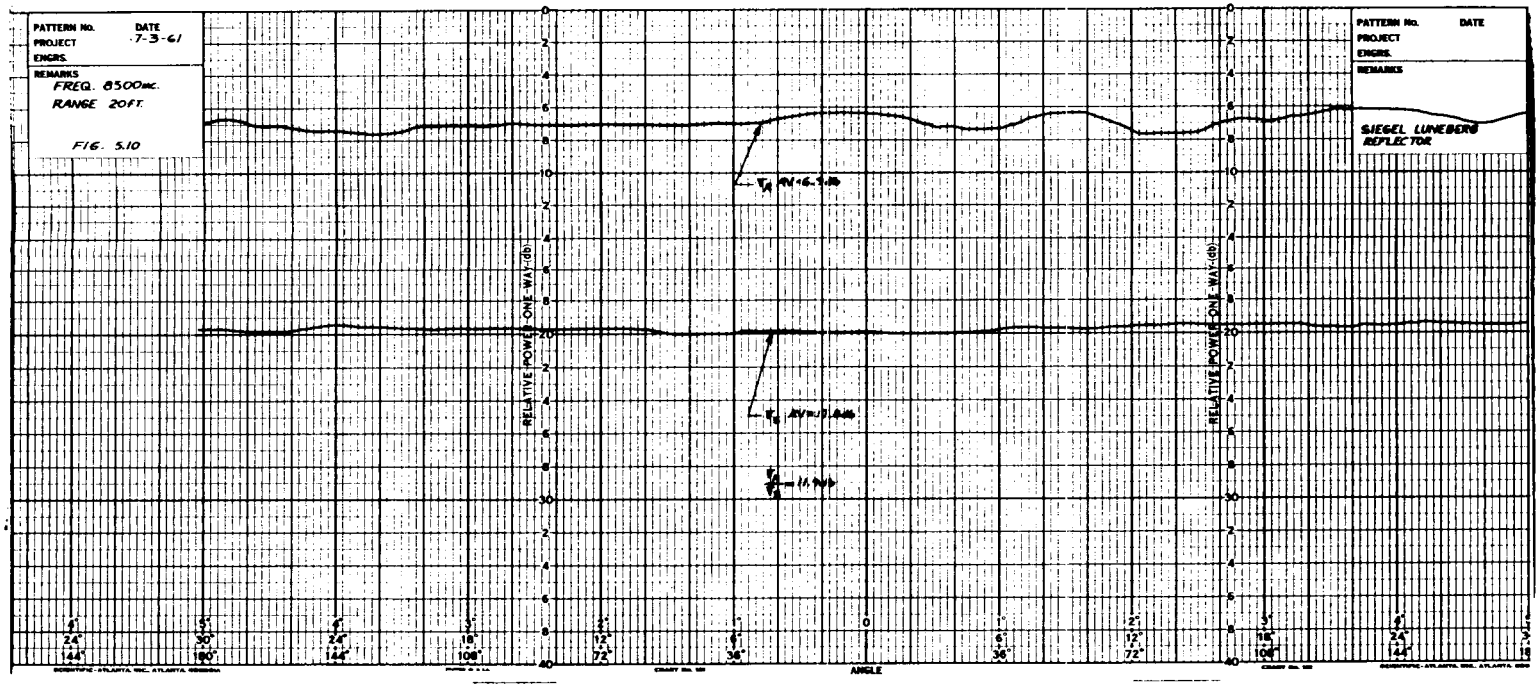
PATTERN No.
DATE 7-3-61
PROJECT
ENGRS.
REMARKS
FREQ. 8500mc.
RANGE 20FT.
FIG. 5.10
PATTERN No.
DATE
PROJECT
ENGRS.
REMARKS
SIEGEL LUNEBERG REFLECTOR
RELATIVE POWER-ONE WAY-(db)
ANGLE

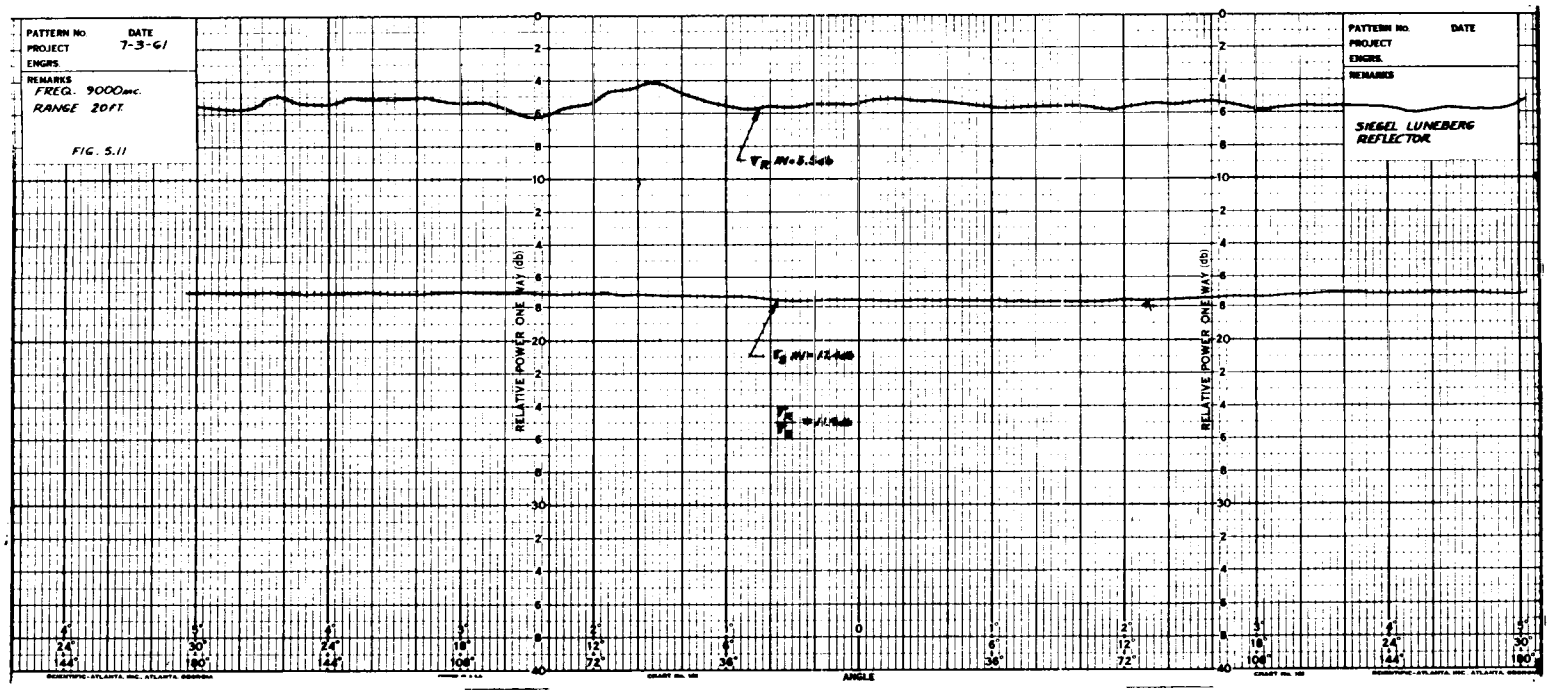
PATTERN NO.
DATE 7-3-61
PROJECT
ENGRS.
REMARKS
FREQ. 9000mc.
RANGE 20ft.
FIG. 5.11
RELATIVE POWER ONE WAY (db)
ANGLE
PATTERN NO.
DATE
PROJECT
ENGRS.
REMARKS
SIEGEL LUNEBERG REFLECTOR

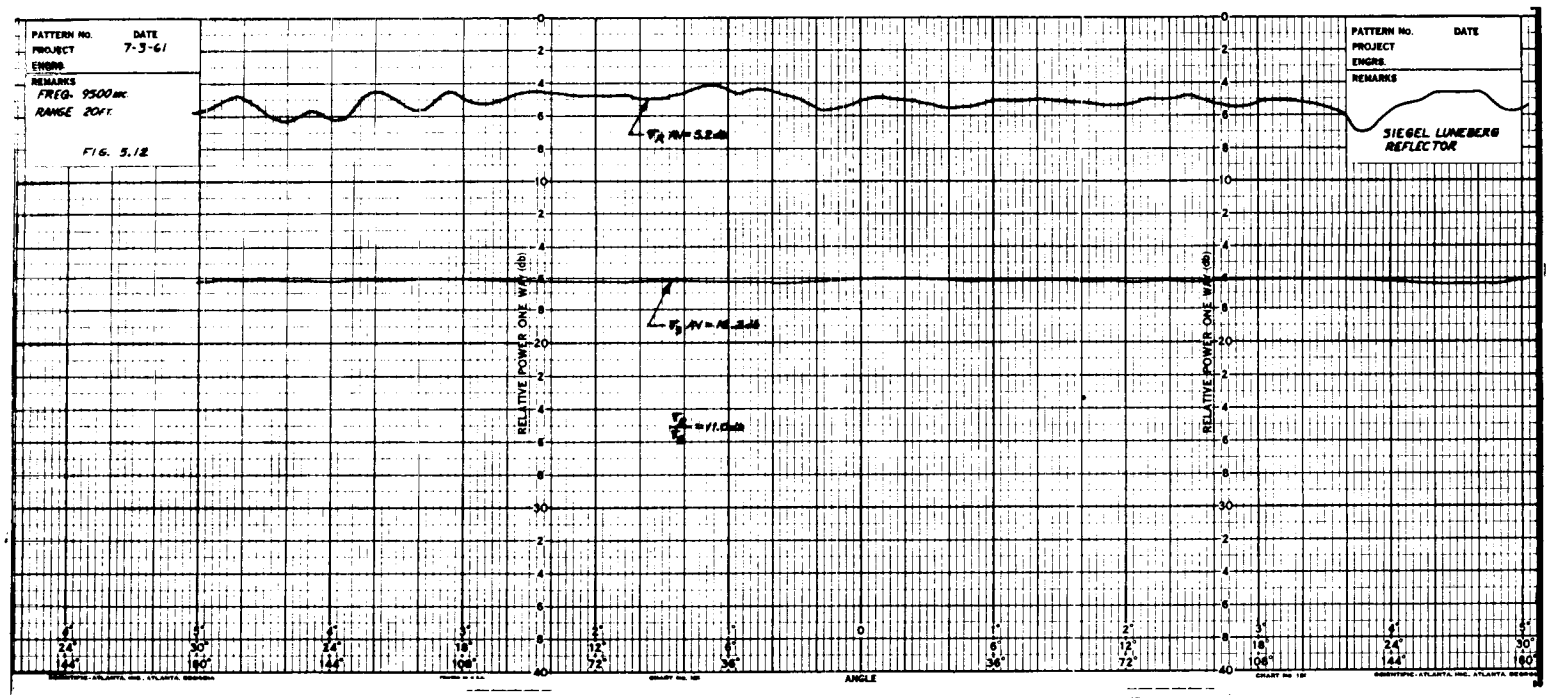
PATTERN NO.
DATE
PROJECT
7-3-61
ENGRS.
REMARKS
FREQ. 9500 mc
RANGE 20 ft.
FIG. 5.12
PATTERN NO.
DATE
PROJECT
ENGRS.
REMARKS
SIEGEL LUNEBERG REFLECTOR
RELATIVE POWER ONE WAY (db)
ANGLE

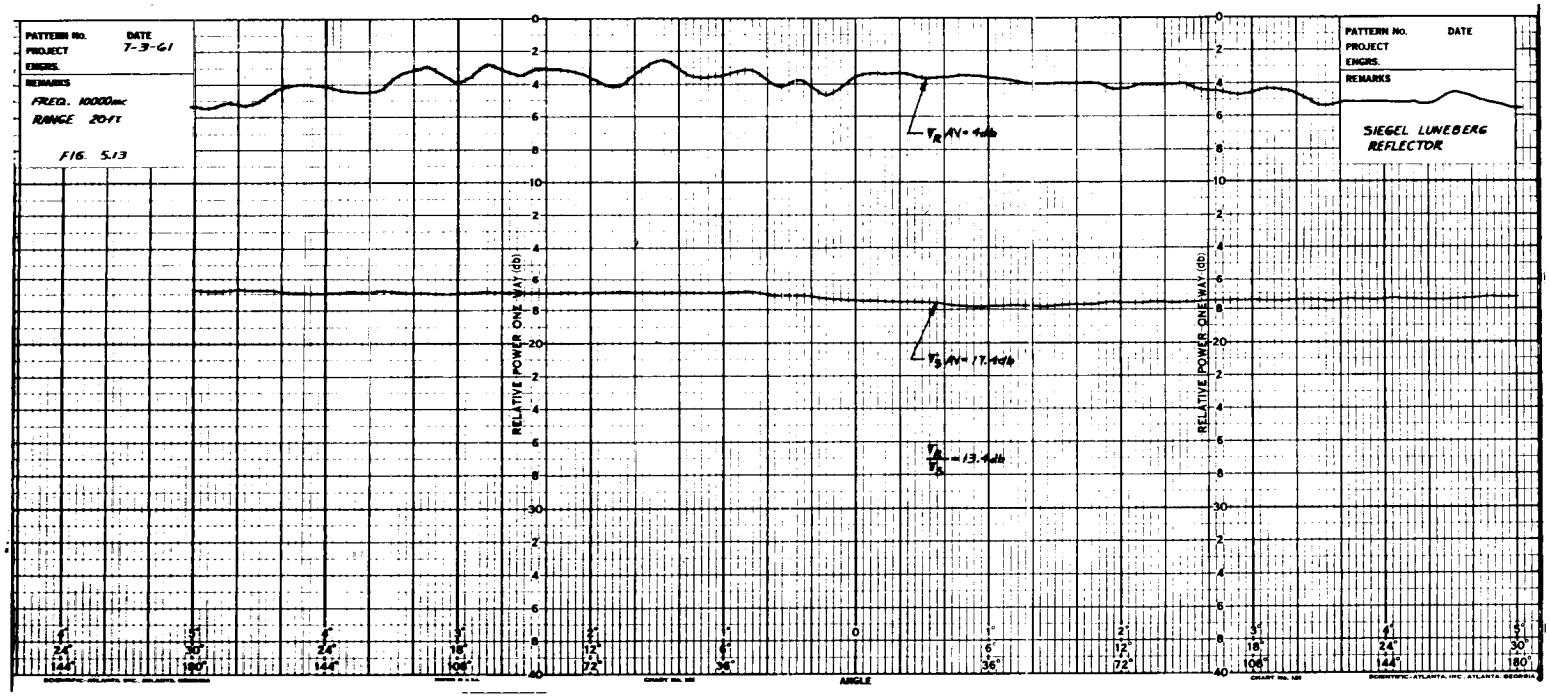
PATTERN No.
DATE 7-3-61
PROJECT
ENGRS.
REMARKS
FREQ. 10000mc
RANGE 20ft
FIG. 5.13
V_R AV = 4db
V_S AV = 17.4db
$\frac{V_R}{V_S}$ = 13.4db
RELATIVE POWER ONE WAY (db)
ANGLE
PATTERN No.
DATE
PROJECT
ENGRS.
REMARKS
SIEGEL LUNEBERG REFLECTOR
SCIENTIFIC-ATLANTA, INC. ATLANTA, GEORGIA

The maximum deviation between the calculated and measured values is 1.8 db which occurs at 9500 mc. This data was rechecked and found to be valid. It is not known exactly why the ratio dips slightly in this region other than it must be a property of the outer coating.

It can be noted from the data that there is a modulation of about ±1 db in the cross section of the reflector. This deviation is somewhat greater at the higher frequencies. This can best be explained by non-uniform spacing between the lens and its outer coating. We would expect this non-uniformity to cause greater errors at the higher frequencies.

The error in our sphere measurements is no greater than ±0.4 db as can be seen by the variation in the cross section of the sphere. This error is caused by background reflections in the anechoic chamber. When this background is taken into consideration for the reflector we calculate that the reflector cross section measurements are in error by no more than ±0.1 db.

Conclusion

In general, the data is in good agreement with the expected results. In future models we hope to improve the construction tolerances and thus reduce the modulation that currently exists. The fact that the present reflector shows good characteristics over the entire X-band region is encouraging. We will take further measurements over wider frequency bands to determine if there are limitations.

We have prepared a chart based on this data and two varieties of commercially available Luneberg lenses which plots the radar cross section and weight of the Siegel Luneberg reflector as a function of diameter for a wavelength of 3.2 cm. The radar cross section of a conducting sphere is also plotted. This chart is shown as figure 5.13 and may be used to a good approximation. Note that for larger reflectors, the gain over perfectly conducting spheres of the same diameter increased directly with the increase in physical area.

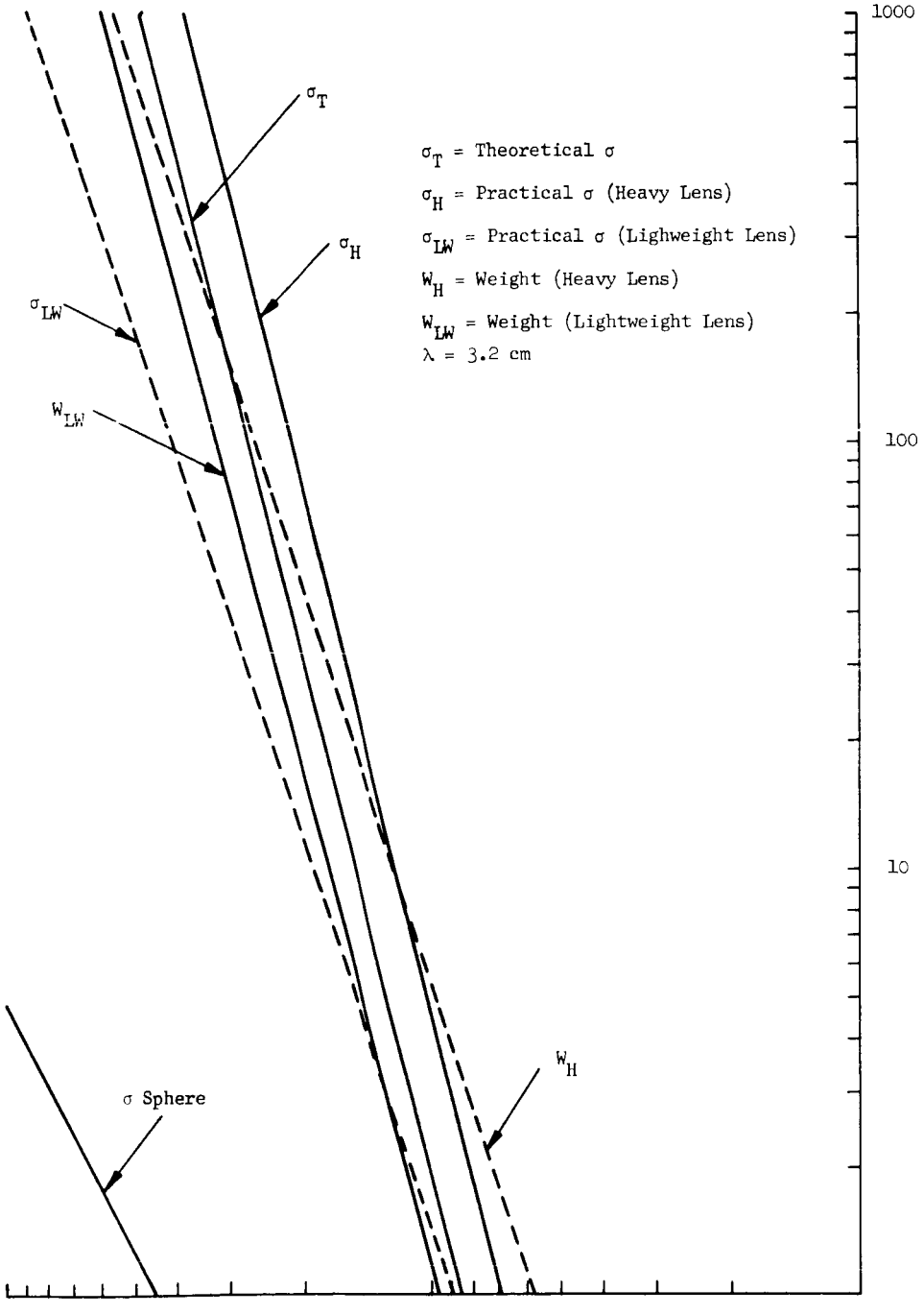

Figure 5.14 Characteristics of Siegel-Luneberg Lens

In the present program,
The 6.5 inch Siegel Luneberg Lens has been measured at several frequencies at both vertical and horizontal polarizations. The following table shows the results in db relative to a 6.5 inch diameter calibration sphere:

Frequency	Db's relative to calibration sphere
970 mc	- 7.0
1300 mc	- 8.0
3.1 kmc	+ 8.0
3.2 kmc	+ 7.8
3.3 kmc	+ 7.5
3.4 kmc	+ 8.0
3.5 kmc	+ 6.75
5.45 kmc	+ 6.5
5.50 kmc	+ 7.5
5.60 kmc	+ 6.0
5.70 kmc	+ 6.8
5.80 kmc	+ 8.2
5.90 kmc	+11.00
5.94 kmc	+11.00

These were insensitive to polarization.

5.2 Lenticular Segments. This section consists of two parts. The first is a theoretical discussion of the cross-section of a spherical segment. This was not done on this program, but is included for completeness. The second is a summary of measurements performed on this program to test this theory.

Nose-on Cross Section of Spherical Segments

The dominant contributions to the nose-on cross section come from the specular reflection and from the diffraction by the edge. The specular reflection gives rise to a cross section independent of wave length. Edge diffraction from a single straight edge gives rise to a field which is of lower order by a factor of $1/\sqrt{k}$. In this problem however, we have

a ring of these contributions and the integration around this loop effectively multiplies this by $\sqrt{k}$, giving a cross section contribution which is independent of k. This change in the frequency dependence arises from the fact that on or near the axis all the edge contributions are in phase whereas the field at a point from the infinite edge, has only a single point on the edge, which is in phase. These two contributions are the leading terms of the asymptotic expansion for large k.

The specular return can be obtained from physical optics and in the far zone is

$$\vec{E}^s = -\vec{E}^{inc} \left(\frac{a}{2r} \right) e^{+ikr - ika}$$

and (5-24)

$$\vec{H}^s = +\vec{H}^{inc} \left(\frac{a}{2r} \right) e^{+ikr - ika}$$

The edge contribution can be obtained from the diffraction by an edge as derived by Sommerfeld. If we restrict ourselves to backscattering and to $\theta < \gamma$, then the total field is given by

$$U = U_o - U^r + G(r,0) \mp G(r,2\alpha) \qquad (5-25)$$

where the upper sign corresponds to the incident electric field along the edge and the lower sign to the incident magnetic field along the edge, and

U_o = incident field

U^r = reflected field

$G(r,2\alpha)$ = diffracted field* = $\dfrac{e^{i(kr + \pi/4)}}{2\sqrt{2\pi\, kr}\, \cos\alpha}$

α = angle of incidence measured with respect to the tangent to the surface at the edge.

---

* This formula doesn't hold for $\theta = \gamma$, since this corresponds to the transition region of half plane solution.

Since we have already taken care of the reflected field, we are interested now in the diffracted field. The above field is that derived for a half plane. The present configuration is a sector of a sphere. As indicated previously we must multiply this by a correction due to the ring of sources all contributing in phase. We do this in the same manner as Siegel, et.al. (Reference 5.8). Considering first, the half plane, the field comes from the edge and thus the scattered field can be represented by an integral of the form

$$U_s = \frac{1}{\lambda} \int U_i \frac{e}{\rho}^{ik\rho} f(\alpha,z)\, dA \qquad (5-26)$$

where U_i is the incident field, ρ is the distance along the propagation direction and A is the area of projection of the part of the scatterer to one side of a plane of constant phase, and $f(\alpha,z)$ is a function which represents the properties of the edge. The field at a point r in the x, y plane for a line source along the z axis gives rise to a scattered field in the far zone of the form

$$U_s = \frac{H_i}{\lambda r} \int_{-\infty}^{+\infty} f(\alpha,z)\, e^{ik\sqrt{r^2 + z^2}}\, dz. \qquad (5-27)$$

This can be evaluated by stationary phase to yield

$$U^s_{2D} = \frac{U_i}{\sqrt{\lambda r}}\, e^{i(kr + \frac{\pi}{4})}\, f(\alpha,\ z = 0) \qquad (5-28)$$

For the three dimensional problem of a finite edge the integral is

$$U^s = \frac{U_i}{\lambda r} \int_0^L f(\alpha,\ z)\ e^{ik\sqrt{r^2 + z^2}}\, dz \qquad (5-29)$$

Reference 8: This formula doesn't hold for $\theta = \gamma$, since this corresponds to the transition region of half plane solution.

which integrates to (for L very small)

$$U^s_{3D} \tilde{\sim} \frac{U_i}{\lambda r} \quad f(\alpha, z) \quad e^{ikr} \, L \tag{5-30}$$

Thus, the Sommerfeld edge answer must be multiplied by the factor

$$F(0) = \frac{L}{\sqrt{\lambda r}} \qquad e^{-i \ \pi/4} \tag{5-31}$$

for nose-on incidence.

Now we must consider the wedge to be of length $a'(d\beta)$ and integrate vectorially around the edge. The total edge diffracted field is

$$\bar{E}^d = \frac{a' \, e^{ikr}}{2(2\pi) \, r} \int_0^{2\pi} d\beta \, \Big| (\hat{\beta} \cdot \bar{E}^{inc}) \hat{\beta} \left(1 - \frac{1}{\cos \alpha}\right) - (\hat{\rho} \cdot \bar{E}^{inc}) \, \hat{\rho} \left(1 = \frac{1}{\cos \alpha}\right) \Big| \tag{5-32}$$

where $\hat{\beta}$ is a unit vector parallel to the edge, $\hat{\rho}$ is a unit vector normal to the edge, and a' is the radius out to the edge. The negative sign between the two contributions arises out of the change in phase at reflection that the E field is subject to.

We can take $\bar{E}^{inc} = -\hat{i}_x$ and

$$\hat{\rho} = -\hat{i}_x \cos \beta - \hat{i}_y \sin \beta$$

$$\hat{\beta} = \hat{i}_x \sin \beta - \hat{i}_y \cos \beta$$

giving

$$\vec{E}^d = \frac{a' \, e^{ikr}}{4 \pi \, r} \int_0^{2\pi} d\beta \, [- \sin \beta \, (\hat{i}_x \sin \beta - \hat{i}_y \cos \beta) \, (1 - \frac{1}{\cos \alpha}) -$$

$$- \cos \beta \, (-\hat{i}_x \cos \beta - \hat{i}_y \sin \beta) \, (1 + \frac{1}{\cos \alpha})] \tag{5-33}$$

$$\vec{E}^{d} = -\frac{a' e^{ikr}}{2r} \qquad \frac{\vec{E}^{inc}}{\cos \alpha} \tag{5-34}$$

Thus, the field due to the edge diffraction is of the same order of magnitude and the same relative sign as the specular field. The total scattered field can be written as

$$\vec{E}^{s} = -\left(\frac{a}{2r} e^{ikr} + \frac{a'}{2r \cos \alpha} e^{ikr} e^{i\delta}\right) \tag{5-35}$$

where δ is the difference in phase between the specular point and the edge points. If we describe our body by the radius a, and the included half angle γ, then

$$a' = a \sin \gamma$$
$$\delta = 2\frac{2\pi}{\lambda} (a - a \cos \gamma)$$
$$\alpha = \frac{\pi}{2} - \gamma$$
$$\cos \alpha = \cos \left(\frac{\pi}{2} - \gamma\right) = \sin \gamma$$

and this reduces to

$$\vec{E}^{s} = -\frac{a}{2r} e^{ikr} \left| 1 + e^{2i\, ka\, (1 - \cos \gamma)} \right| \tag{5-36}$$

and the nose-on radar cross section is

$$\sigma = 4\pi a^2 \cos^2 ka\,(1-\cos \gamma) \tag{5-37}$$

Near Nose-On Cross Section

In this section we determine the cross section of the dish configuration in the near nose-on region. More precisely, we will determine the cross section in a region such that

$$\sin \theta >> \frac{1}{2\, ka'} \qquad (a' = a \sin \gamma)$$

and

$$\theta < \gamma.$$

This region is characterized by the following:

a. specular reflection is present

b. all of edge in "lit" region

c. the entire edge is <u>not</u> in phase at any angle.

To evaluate the effect of the edge diffraction, we shall again use the Sommerfeld straight result. However, in this case it is clear that the multiplying factor used to transform must take on a different form. In the nose-on case, all edge currents contributors were in phase. In this case, there will be considerable variation in phase as we integrate around the ring. For high frequencies, we expect that the major contributions will come from those points at which the phase is stationary. To see this let us again refer to the integral expression for the scattered field, namely,

$$U_s = \frac{1}{\lambda} \int_s U_i \frac{e^{ik\rho}}{\rho} f(\alpha,z)\, dA. \qquad (5-38)$$

For the infinite straight edge we again get

$$U^s_{2D} = \frac{U_i}{\sqrt{\lambda r}} e^{i(kr + \pi/4)} f(\alpha,\ z = 0) \qquad (5-39)$$

Now we consider a ring discontinuity in the x, y plane. The corresponding integral is now

$$U^s_{3D} = \frac{1}{\lambda r} \int_s U_i\ e^{ik\rho}\ f(\alpha,\ \phi')\, dA \qquad (5-40)$$

and

$$\rho = -(a' \sin\theta \cos\phi' + a' \sin\theta \sin\phi \sin\phi')$$

The ϕ' integration can be performed by stationary phase, provided $2ka' \sin\theta >> 1$. For the parameters of interest here, namely, ka 6π(70Gc/s) and

3π (35 Gc/s), this requires $\theta >> 4^{o}$ and $\theta >> 6^{o}$. Using stationary phase we find that there are two stationary points, namely, respectively, $\phi' = \phi$ and $\phi' + \pi$. The result of the ϕ' integration is then

$$U^{s}_{3D} = \sqrt{\frac{a}{\lambda \sin\theta}}\, U_3\, e^{\mp \frac{\pi}{4} i}\, \frac{e^{ikr}}{r}\, f\left(\alpha, \phi' = \begin{cases} \phi \\ \phi + \pi \end{cases}\right) \qquad (5\text{-}41)$$

where r is the distance from the field point to the stationary point, the upper sign corresponds to the point $\phi' = \phi + \pi$ and the lower sign to the point where $\phi' = \phi$. Thus, we conclude that the field from the Sommerfeld straight edge must be multiplied by

$$F\left(\phi' = \begin{cases} \phi \\ \phi + \pi \end{cases}\right) = \mp \sqrt{\frac{a}{r \sin\theta}} \qquad (5\text{-}42)$$

to give the edge contributions for our problem.

Referring to Figure 5.15 for the case $\phi' \neq \phi$ we see that the distance from a plane of constant phase through the origin to the edge is

$$d_1 = a \cos(\gamma - \theta), \qquad (5\text{-}43)$$

$a' = a \sin\gamma$ and the angle made by the ray with the tangent to the surface is

$$\alpha_1 = \frac{\pi}{2} - (\gamma - \theta) \qquad (5\text{-}44)$$

Similarly, from Figure 5.15 , we have

$$d_2 = a \cos(\gamma + \theta) \qquad (5\text{-}45)$$

$$\alpha_2 = \frac{\pi}{2} - (\gamma + \theta) \qquad (5\text{-}46)$$

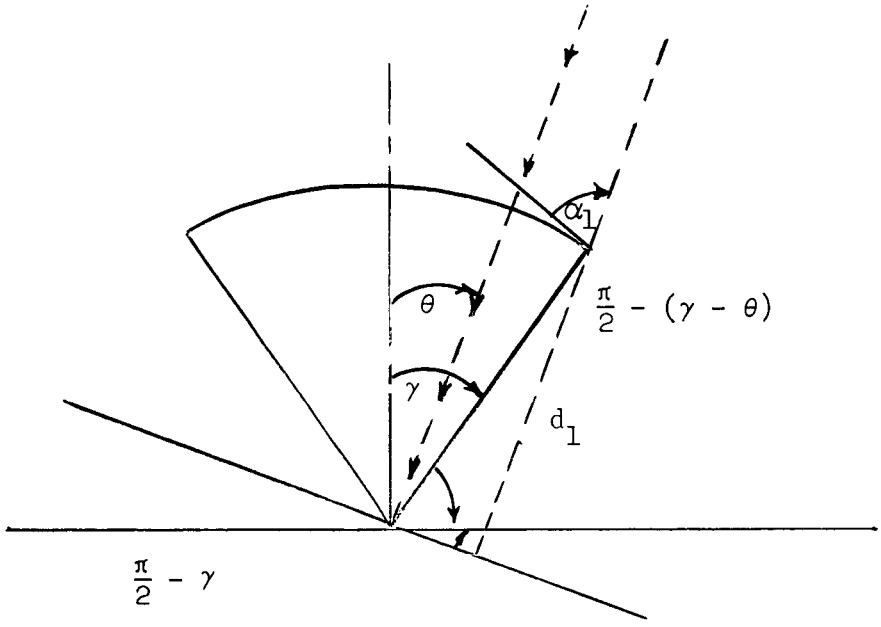

Parameters for $\phi' = \phi$

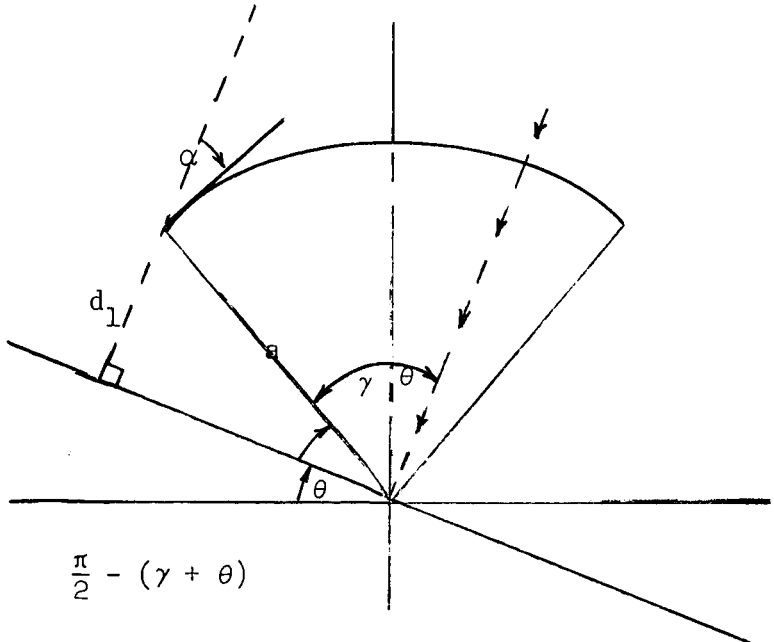

Figure 5.15

Parameters for $\phi' = \phi + \pi$

Using expression (5.42) with the Sommerfeld edge results, we have for the edge diffracted terms

$$U^s = \frac{-e^{i(kr + \pi/4)}}{2r} \sqrt{\frac{a}{2\pi\, k \sin\theta}} \left\{ e^{-2i\, ka \cos(\gamma - \theta)} \left| 1 \mp \frac{1}{\sin(\gamma - \theta)} \right| \right.$$

$$\left. - e^{-2ika \cos(\gamma + \theta)} \left| 1 \mp \frac{1}{\sin(\gamma + \theta)} \right| \right\} \quad (5\text{-}47)$$

where the upper sign corresponds to $\vec{E}$ tangent to edge at $\phi' = \phi,\ \phi + \pi$ (vertical polarization) and the lower sign corresponds to $\vec{H}$ tangent to edge at $\phi' = \phi,\ \phi + \pi$ (horizontal polarization). It is important to remember that this expression is valid only for $\theta < \gamma < \frac{\pi}{2}$. To this we add the specular contribution, namely

$$U = \mp\ a\ \frac{e^{i(kr - 2\,ka)}}{2r}$$

Thus, the cross section is

$$\sigma_{h} = \pi\, a^2 \left| 1 - \frac{1}{\sqrt{2\pi\, ka \sin\theta}} \right.$$

$$\left. e^{2in\eta_1} \left(1 \mp \frac{1}{\sin\gamma - \theta}\right) - e^{2i\,\eta_2} \left(1 \mp \frac{1}{\sin\gamma + \theta}\right) \right|^2 \quad (5\text{-}48)$$

where $\eta_1 = ka\ [1 - \cos(\gamma - \theta)]$

$\eta_2 = ka\ [1 - \cos(\gamma + \theta)]$

Experimental Results

Previously, the static cross section of a spherical segment large compared with wavelength was determined as a function of the size of the segment, aspect and polarization. To check on the accuracy of this evaluation a series of measurements were performed at X band frequencies on scale models. The measurements were not intended as a systematic precision experiment, but rather a spot check at key values to demonstrate the validity of the theory. The experiments do indicate that the magnitudes of these contributions are correct but there appears to be a phase error of the order of $\frac{\pi}{4}$.

Models:

The models were made of aluminum 12 thousands of an inch thick and to an accuracy of approximately 1/10" or $\lambda/10$. The models were made by spinning the aluminum over a wood mold on a standard wood lathe. This method of fabrication was chosen purely on a basis of cost. Models made in this manner can be made quickly and inexpensively, whereas precision models would have been very expensive. Inaccuracy of the experiment due to model deviations can be expected to be less than 1/2 db.

Several models were made, each having a different intersecting angle γ (see Fig. 5.16A) The height, h, for each model was given by

$$h = \frac{7}{12} N \text{ inches}$$

where N had the values 2, 2.5, 3, 3.5, 4.0 and 4.5. Each body is labeled by its value of N. The radius of curvature in each case was 3 1/2 inches. Thus at 10.15 Kmc, $kh = N\pi$ so $2\pi \geq kh \geq 4.5\pi$ and $ka = 6\pi$. The angle γ for various N is given in Table 5.3.

N	γ
2.0	$48\ 1/5^{o}$
2.5	$54\ 2/5^{o}$
3.0	60^{o}
3.5	$65\ 2/5^{o}$
4.0	$70\ 1/2^{o}$
4.5	$76\ 2/3^{o}$

Measurements:

Measurements were made at X band frequencies between 8.5 kmc and 10.0 Kmc.

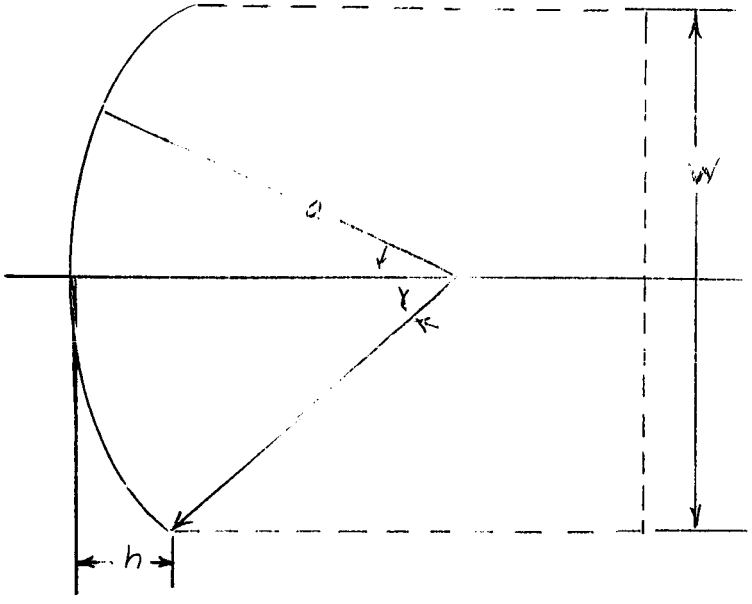

Figure 5.16A Model Geometry

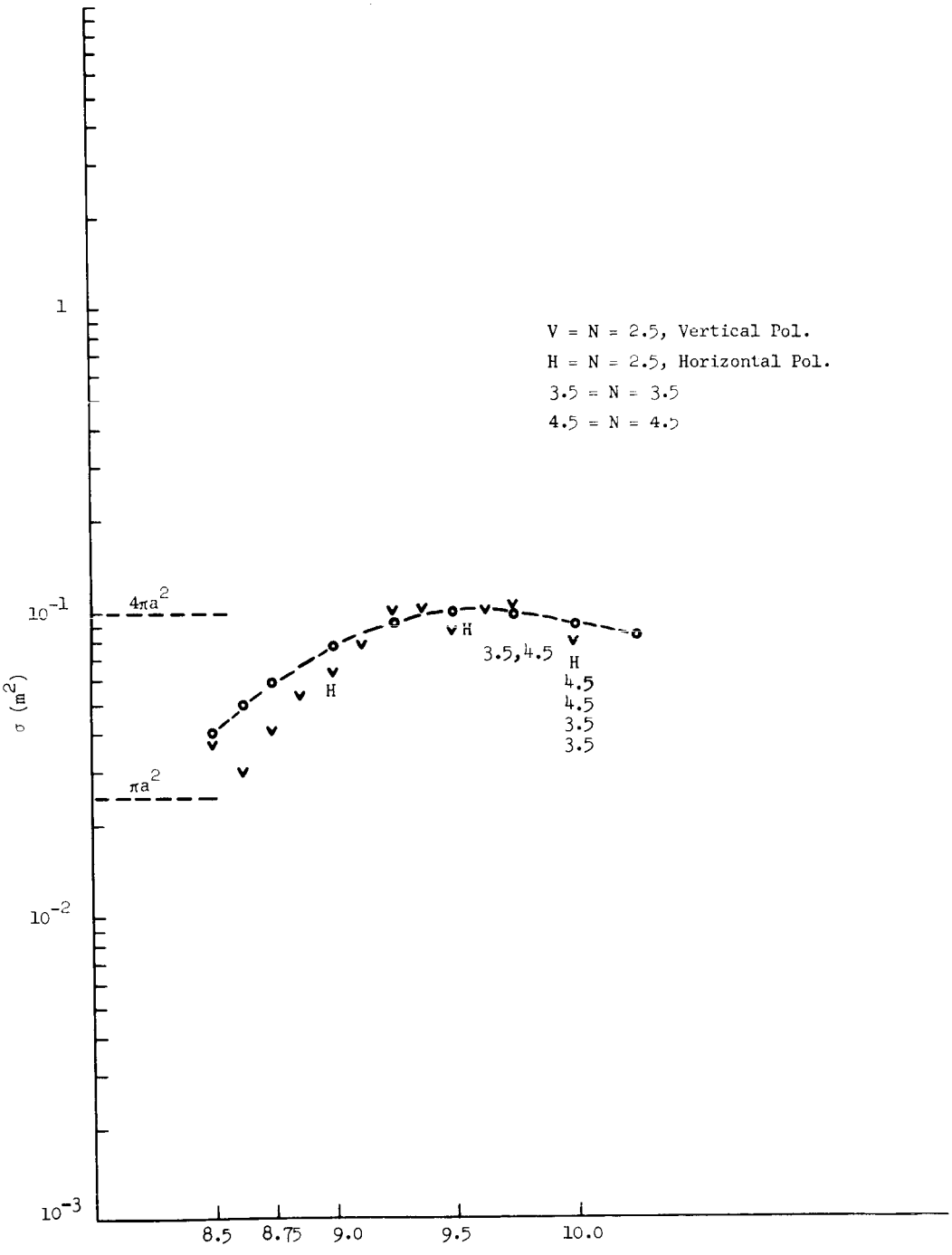

Figure 5.16 Nose-On Cross Section Vs. Frequency When N Has Half Integer Values

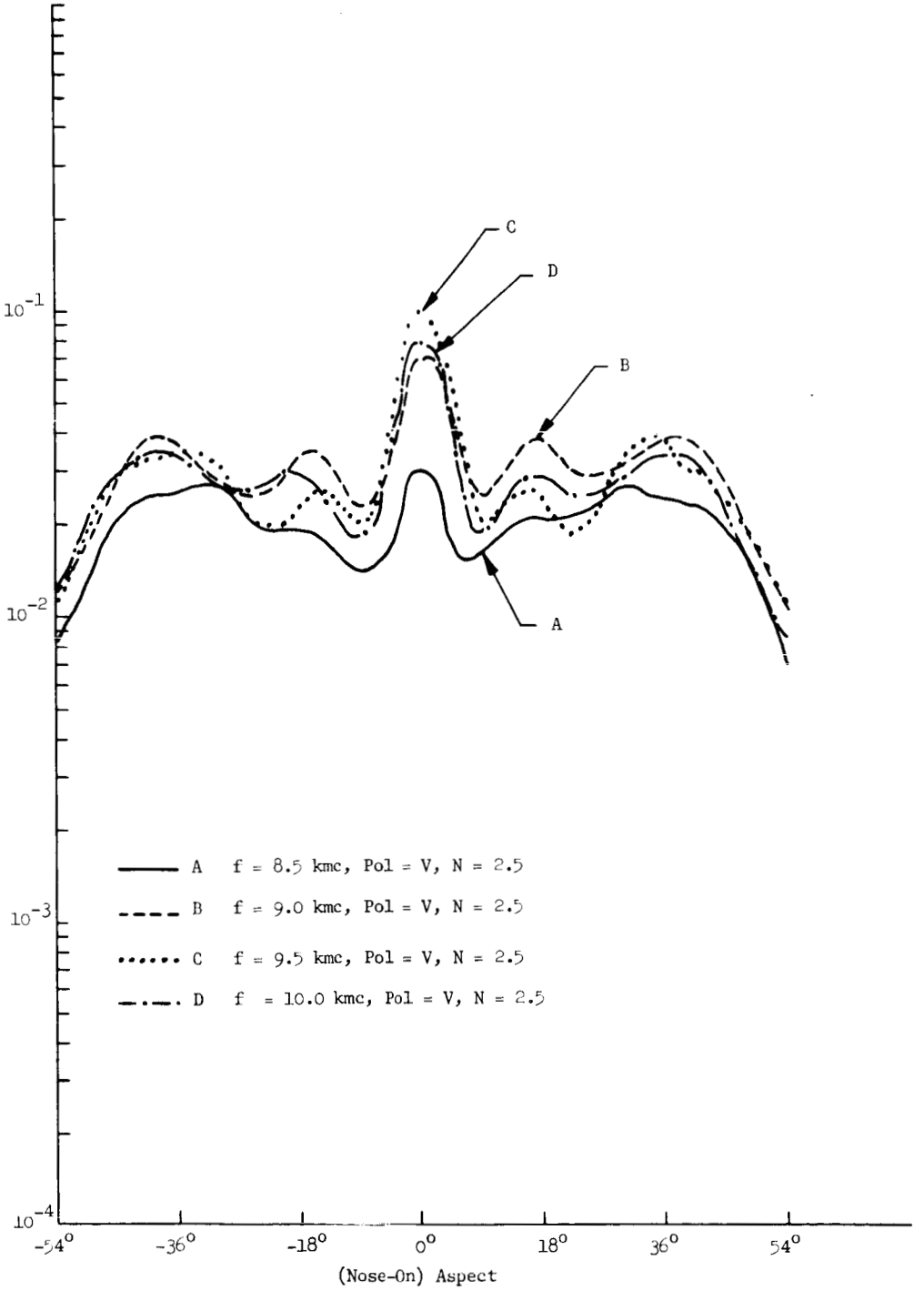

Figure 5.17 Cross Section Vs. Aspect For N = 2 1/2 Spherical Segment

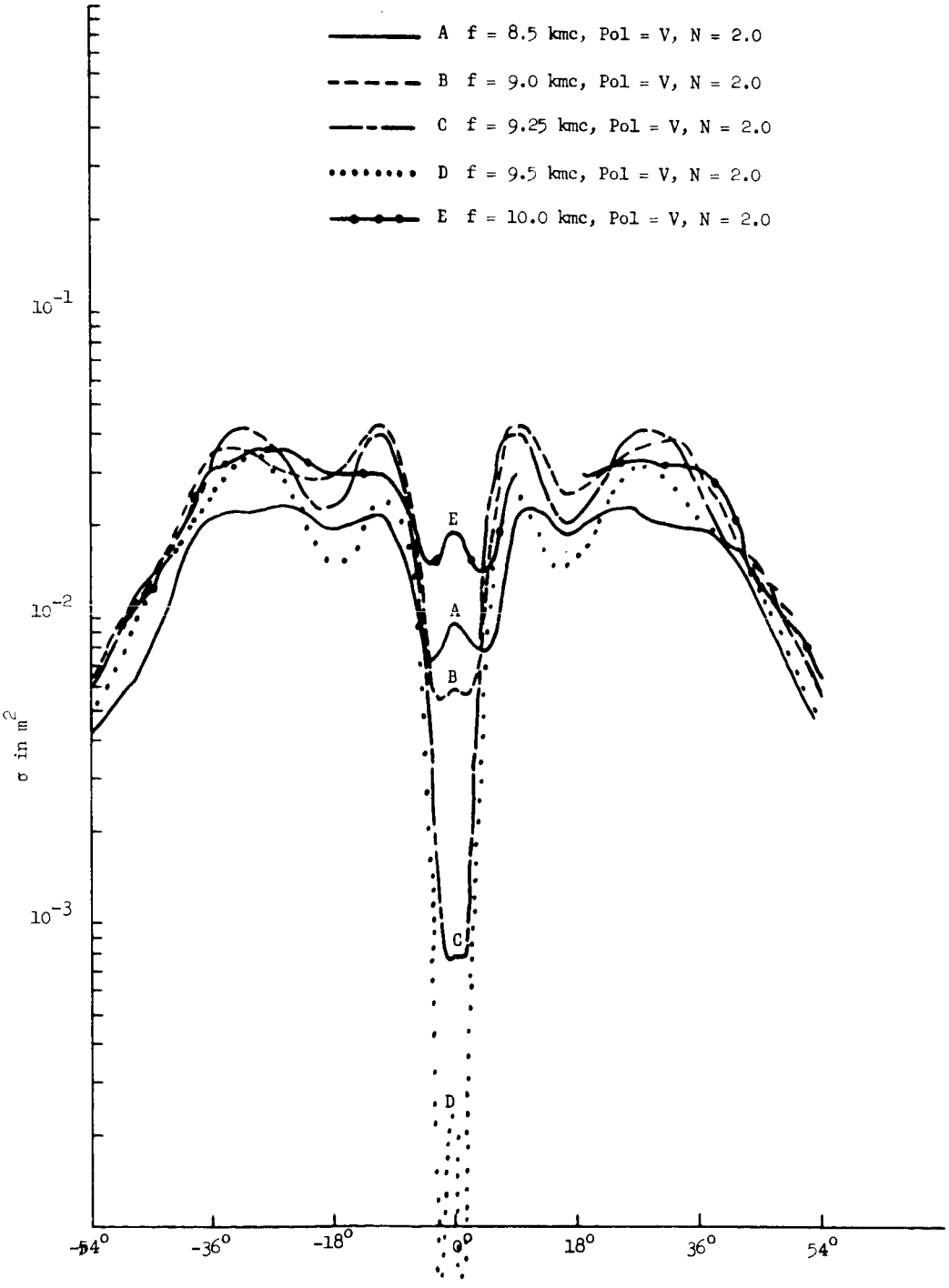

Figure 5.18 Cross Section Vs. Aspect For N = 2.0 Spherical Segment

For N = 2.0 and 2.5, measurements were made at several intermediate frequencies and for the other models, measurements were made at only 9.5 and 10 Kmc. Measurements were made at horizontal and vertical polarizations, but not all measurements were made at both polarizations.

Calibrations were made on a 3.5" diameter sphere whose cross section was read from a 15" x 15" semi log plot of cross section vs. frequency. Reading errors from the calibration chart in this region are as large as a 1/2 db. Background levels were kept to a level of about -50 dbM. Better backgrounds are of course possible, but except for certain nulls, these measurements were quite adequate.

The far zone criteria of the range being greater than

$$R > \frac{2\ D^2}{\lambda} = 4 \text{ ft.}$$

was satisfied by using a range of 7 1/2 feet throughout.

Results:

Fig. 5.16 gives the nose-on cross section in M^2 vs. frequency for the spherical segments when N assumed half integer values. Based on the derived formula, namely

$$\sigma = 2\pi\ a^2\ [\ 1 + \sin 2\ ka\ (\ 1 - \cos\ \gamma\ )\ ]$$

the value of σ should be $\sigma = 5 \times 10^{-1}\ M^2$ at f = 10.15 Kmc for each value of N. Actually there appears to be a phase error of $\frac{\pi}{4}$ and the data fits a curve given by

$$\sigma = 2\pi\ a^1\ [\ 1 + \sin\ \{2\ ka\ (1 - \cos\ \gamma) - \tfrac{\pi}{4}\ \}\ ]$$

We note that the amplitude at peak values is predicated accurately and there is small error in other values.

Fig. 5.17 gives a graph of cross section vs. aspect for various frequencies for the N = 2 1/2 spherical segment. We note the characteristic curve for a function which has two contributors going in phase. Fig. 5.18 gives the same curves but for the N = 2.0 spherical segments. We note that at nose-on the null is down by 27 db. and undoubtedly be lower if finer frequency intervals

were used. Fig. 5.19 gives a comparison of two extreme cases. This proves that the two contributors are equal in magnitude at nose-on. Off nose-on the magnitudes are not equal. This is precisely as predicted theoretically.

Theoretically it was also predicted that off nose-on there would be a polarization dependence to the cross section. Fig. 5.20 & 5.21 show the effect of different polarizations. We note that at 9^{o} there is of the order of 4 db difference between horizontal and vertical polarizations. From Fig. 5.21, we also observe that at certain situations (particularly deep nulls) there is an extreme sensitivity to aspect. In particular one notes a 6 db change over 1^{o} aspect change and a 26 db change over a 9^{o} aspect change. For situations near peaks (Fig. 5.20) we observe only 10 db change over 8^{o} aspect change at vertical polarization and 6 db change over 8^{o} aspect change at horizontal polarization.

Conclusions:

The experimental data demonstrates the basic validity of theoretical analysis in predicting

a) there are two contributions to the cross section at nose-on; one from the specular contribution, the other from the ring discontinuity at the edge.

b) these contributions are equal in magnitude.

c) the cross section near nose-on is polarization dependent.

The experiments also demonstrate that there is an error in calculated theoretical phase, most likely of the order of $\pi/4$. A check of the phases indicate that the phase of the edge term is essentially the same as obtained by both Siegel and Keller (Reference 9 and 10) for the finite cone, which has a wedge discontinuity of a similar nature. A possibility exists that the error is essentially algebraic or due to the use of the Kirchhoff integral.

Usually in scattering problems a phase factor of this type is insignificant. We note in this case that the phase is very important in that the value of n (index of refraction of plasma) for which the nulls occur in the proposed explanation of the experiment is based on the actual values of the phase. Thus we see that the value of n previously derived in memo 1520-3-M is wrong.

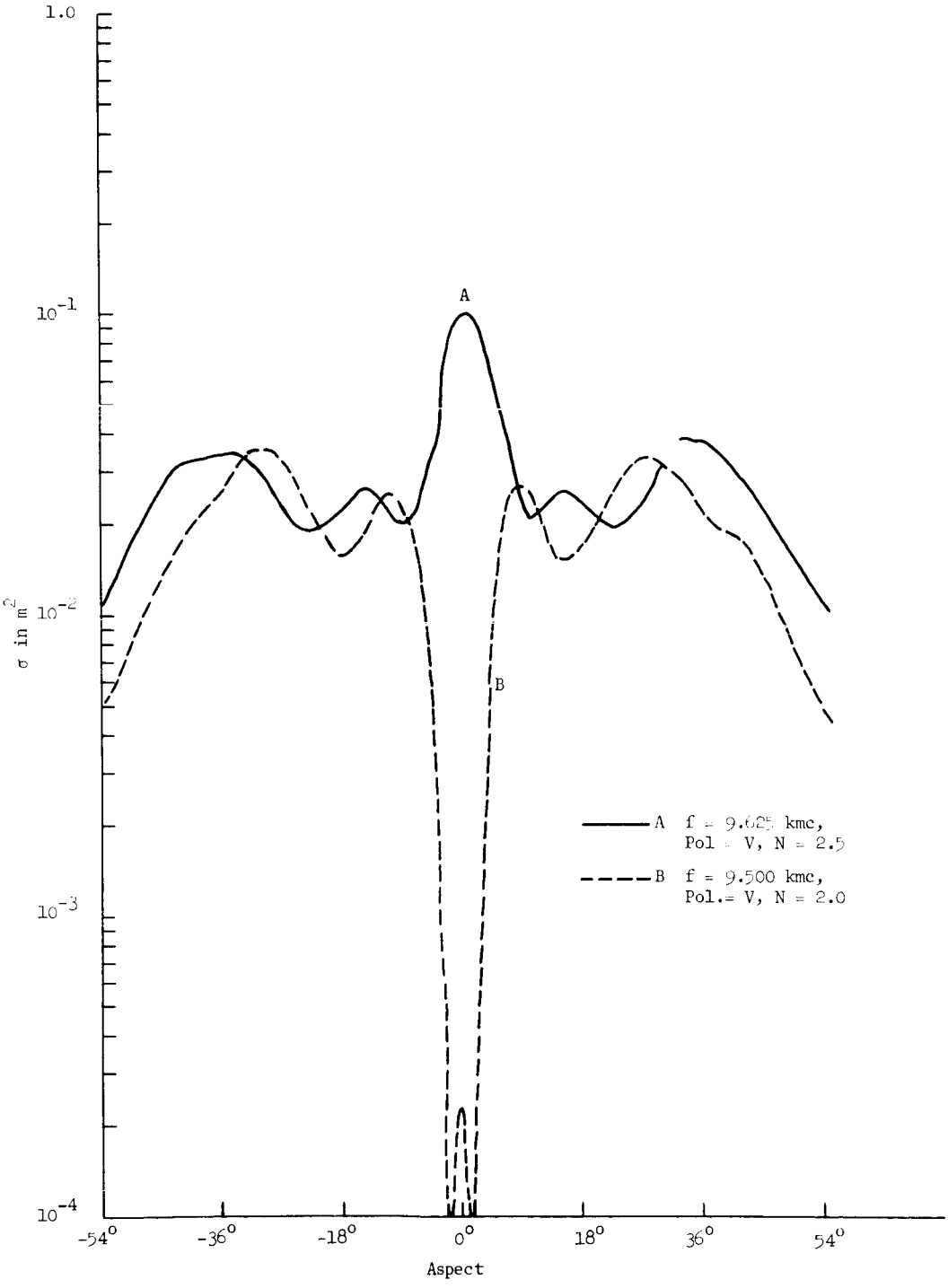

Figure 5.19 Cross Section Vs. Aspect for Two Extreme Cases

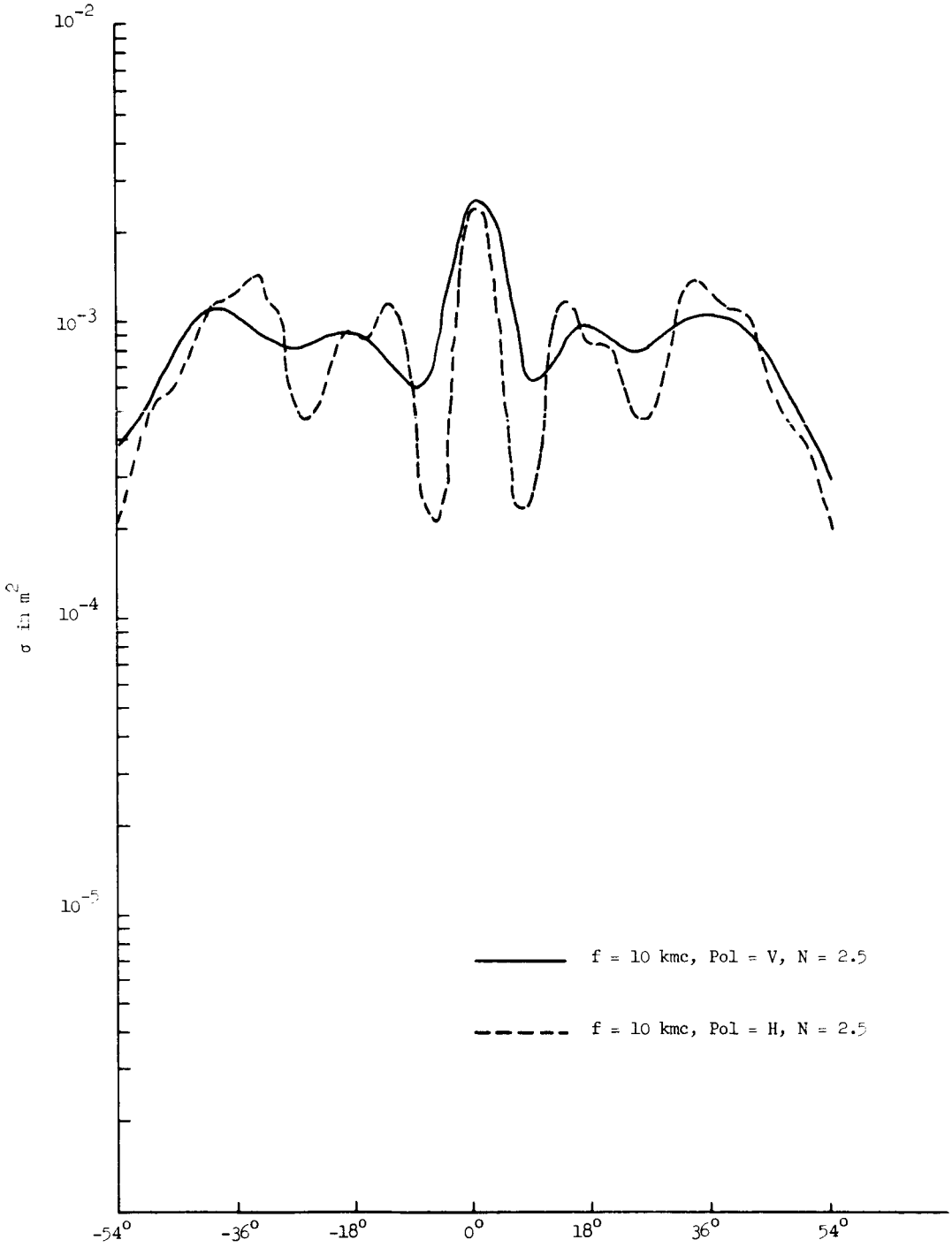

Figure 5.20 Cross Section Vs. Aspect at Two Polarizations

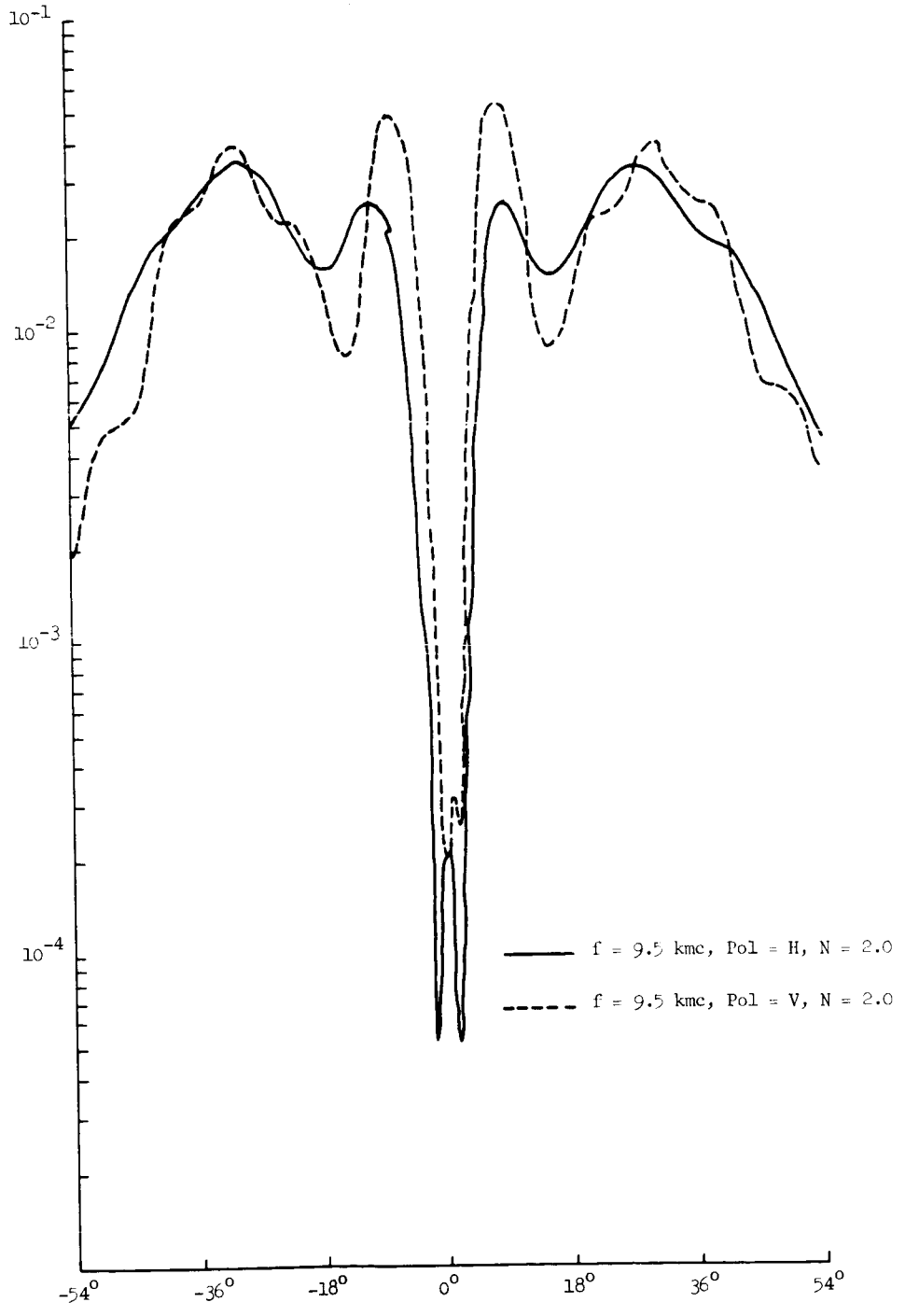

Figure 5.21 Cross Section Vs. Aspect at Two Polarizations

5.3 Diffuse Scattering Mechanisms

A large number of authors have estimated that by using a large number of reflectors on a sphere, radar cross section enhancement can be obtained. In this section we shall discuss two such mechanisms. The first is the placement of resonant dipoles uniformly, with random orientation on the surface of the sphere. Although this idea is not new, there does not seem to be an adequate description of its effect in the literature.

Scattering from a Dipole

In a standard spherical coordinate system, a half wave dipole, operating in its resonant mode and oriented in the z direction will have a radiation field, $[\underline{E}, \underline{H}]$ given by

$$\begin{aligned} \underline{E} &= \frac{\dot{z}I}{z\pi} F(\theta)\frac{e^{ikR}}{R}\hat{\theta} \\ \underline{H} &= \frac{\dot{z}I}{z\pi} F(\theta)\frac{e^{ikR}}{r}\hat{\varphi} \end{aligned} \tag{5-49}$$

where

$$F(\theta) = \frac{\cos\left(\frac{\pi}{2}\cos\theta\right)}{\sin\theta} \tag{5-50}$$

R = radial distance, I = maximum current amplitude, and $\hat{\theta}$ and $\hat{\varphi}$ are the usual unit vectors. If an incoming plane wave is incident upon the dipole, with direction of incidence θ_0, and polarization p_0, $[(\hat{p}_0 \cdot \hat{\theta}_0) = 0]$, for large values of R, the total field is

$$\begin{aligned} \underline{E} &= e^{-ik\hat{u}_0\cdot\vec{v}}\hat{p}_0 + \frac{\dot{z}I}{z\pi} F(\theta)\frac{e^{ikR}}{R}\hat{\theta} \\ \underline{H} &= e^{-,k\hat{u}_0\cdot\vec{v}}(\hat{p}_0 \times \hat{u}_0) + \frac{\dot{2}I}{2\pi} F(\theta)\frac{e^{ikR}}{R}\hat{\varphi} \end{aligned} \tag{5-51}$$

The energy flux in the radial direction is then

$$\text{Real part } [\underline{E} \times \underline{\tilde{H}}] \cdot \hat{r} =$$

$$(\hat{u}_0 \cdot \hat{\pi}) + \frac{I^2}{u\pi R^2} (F(\theta))^2 + \frac{iI}{4\pi} \frac{F(\theta)}{R} [\hat{p}_0 \cdot \hat{\theta} + \hat{\varphi} \cdot (\hat{p}_0 \times \hat{u}_0)] \cdot [e^{ikR(1+\hat{u}_0 \cdot \tilde{r})} - e^{-1kR(1+\hat{u}_0 \cdot \tilde{r})}] \quad (5\text{-}52)$$

The conservation of energy dictates that the total energy flux across a large sphere be zero, or

$$\frac{I^2}{4\pi^2} \int\int^{2\pi,\pi} (F(\theta)^2 \sin\theta d\theta d\varphi = \frac{IR}{2\pi} dm \left\{ \int\int e^{ikR(1+\hat{u}_0 \cdot \hat{r})} F(\theta) [\hat{p}_0 \cdot \hat{\theta} + \hat{\varphi} \cdot (\hat{p}_0 \times \hat{u}_0)] \sin\theta d\theta d\varphi \right\} \quad (5\text{-}53)$$

Integration of (53), and letting $R \to \theta$, gives

$$\frac{I^2}{4\pi^2} \int_0^{\pi} (F(\theta))^2 \sin\theta d\theta = \frac{2I}{k} F(\theta_0))\hat{p}_0 \cdot \hat{\theta}_0),$$

or

$$I = \frac{4\pi}{k} \frac{F(\theta_0) (\hat{p}_0 \cdot \hat{\theta}_0)}{\int^{\pi} (F(\theta))^2 \sin\theta d\theta} \quad (5\text{-}54)$$

Therefore, the scattered electric field, using (5-49) and (5-54) is

$$\underline{E}^{sc} = \frac{zi}{k} \frac{F(\theta) F(\theta_0)}{\int_0^{\pi} (F(\theta))^2 \sin\theta d\theta} (\tilde{p}_0 \cdot \tilde{\theta}_0) \frac{e^{ikR}}{R} \theta \quad (5\text{-}55)$$

Now consider a surface with generic point $\vec{r}$. Let U_o and U be the directions of the incident and scattered field, and let $\hat{z}$ be a unit vector on the surface, lying in the tangent plane. In terms of the preceding discussion,

$$\cos\theta_o = (\hat{z}\cdot\hat{U}_o) \ , \quad \cos\theta = (\hat{z}\cdot\hat{U}),$$

$$\hat{\theta}_o = \frac{(\hat{U}_o\cdot\hat{z})\,\hat{U}_o - \hat{z}}{\sin\theta_o} \ , \quad \frac{\hat{\theta} = (\hat{U}\cdot\hat{z})\,\hat{U}-\hat{z}}{\sin\theta} \ ;$$

if $\hat{q}$ is a unit vector, $\hat{q}\cdot\hat{U} = 0$, the component of the scattered field in the direction $\hat{q}$ is:

$$E_q^{sc} = \frac{zi}{k}\left[\frac{\cos(\pi/2\cos\theta)}{\sin^2\theta} \quad \frac{\cos(\pi/2\cos\theta_o)}{\sin^2\theta_o}\right](\hat{p}_o\cdot\hat{z})(\hat{q}\cdot\hat{z})$$

$$e^{-ik\vec{r}\cdot(\hat{U}+\hat{U}_o)} \ \frac{e^{ikR}}{R}\int_o^{\pi}\frac{[\cos(\pi/2\cos\theta)]^2}{\sin\theta}\,d\theta \qquad (5\text{-}56)$$

Since $\hat{z}$ is in the tangent plane we can write

$$\hat{z} = (\sin\alpha)\,\hat{e}_1 + (\cos\alpha)\,\hat{e}_2,$$

where $\hat{e}_1$ and $\hat{e}_2$ are two fixed orthogonal vectors in the tangent plane. Then

$$\begin{aligned}(\hat{p}_o\cdot\hat{z})\,(\hat{q}\cdot\hat{z}) &= \sin^2\alpha\,(\hat{e}_1\cdot\hat{p}_o)\,(\hat{e}_1\cdot\hat{q}) \\ &+ \sin\alpha\cos\alpha\,[(\hat{e}_1\cdot\hat{p})\,(\hat{e}_2\cdot\hat{p}_o) + (\hat{e}_2\cdot\hat{p}_o)\,(\hat{e}_1\cdot\hat{q})] \\ &+ \cos^2\alpha\,(\hat{e}_2\cdot\hat{p}_o)\,(\hat{e}_2\cdot\hat{q}) \qquad (5\text{-}57)\end{aligned}$$

Using numerical integration, the quantity $\int_o^{\pi}\frac{(\cos\pi/2\cos\theta)^2}{\sin\theta}\,d\theta$ can be approximated by 6/5. Then thinking of the dipoles as being uniformly distributed, but with random orientation, on the surface of a sphere, with random, but uniform, orientation, the total q component of the scattered field is

$$E_q \sim \frac{5\dot{z}}{3k} \rho a^2 \frac{e^{ikR}}{R} \iint G(\vec{r}) \, e^{-ik\vec{r} \cdot (\hat{U}+\hat{U}_o)} \, dr \qquad (5\text{-}58)$$

where ρ = number of dipoles | unit area, a = radius of sphere, the integral is extended over the illuminated portion of the sphere, and $G(\vec{r})$ is the random variable:

$$G(\vec{r}) = \left[\frac{\cos(\pi/2 \cos\theta)}{\sin^2\theta}\right] \left[\frac{\cos(\pi/2 \cos\theta_o)}{\sin^2\theta_o}\right] (\hat{p}_o \cdot \hat{z}) (\hat{q} \cdot \hat{z}) \qquad (5\text{-}59)$$

If the sphere is located at the center of an (X, Y, Z) coordinate system, let

$$\left.\begin{aligned} \hat{U}_o &= \varphi \hat{Z} \\ \hat{U} &= \text{sim}\,\beta \hat{\underline{X}} + \cos\beta \hat{Z}, \\ \hat{p}_o &= \hat{\underline{X}}, \quad \hat{q} = \cos\beta \hat{\underline{X}} - \text{sim}\,\beta \hat{Z}, \end{aligned}\right\} \qquad (5\text{-}60)$$

where

β is the <u>bistatic angle</u>. Then, evaluating the integral (57) by stationary phase, assuming $ka \gg 1$, we obtain

$$E_q \sim \frac{-5}{12\pi} [\rho \lambda^2] \frac{a}{\cos\beta/2} G(\vec{r}_s) \frac{e^{1kR}}{R} \qquad (5\text{-}61)$$

where $\vec{r}_s$ is the stationary phase point,

$$\vec{r}_s = a\,[\text{sim}\beta/2\, \hat{\underline{X}} + \cos\beta/2\, \hat{Z}] \qquad (5\text{-}62)$$

The expected value of the cross section is then

$$\langle\sigma \sim (\pi a^2) \left|\frac{5}{12\pi} \rho \lambda^2\right| \frac{4}{\cos^2\beta/2} \langle | G(\vec{r}_s)|^2 \rangle \qquad (5\text{-}63)$$

Recalling (56) we can now find the expected value of $|G(\vec{r}_s)|^2$ by evaluating the integral

$$\frac{1}{2\pi}\int_0^{2\pi} |G(\vec{r}_s)|^2 \, d\alpha \qquad (5\text{-}64)$$

where $G(\vec{r}_s)$ is given by (58). To evaluate (58) we first observe that the quantity $\frac{\cos(\pi/2 \cos\theta)}{\sin^2\theta}$ ranges, in value, between $\frac{\pi}{4}$ and 1. We shall therefore replace the integral (64) by

$$\frac{p^2}{2\pi}\int_0^{2\pi} [p_o\cdot\hat{z})\ (\hat{q}\cdot\hat{z})]^2 \, d\alpha, \qquad (5\text{-}65)$$

in which $\frac{\pi}{4} < \gamma < 1$. Using (56) the fact that

$$\hat{p}_o = (\hat{p}_o\cdot\hat{e}_1)\ \hat{e}_1 + (\hat{p}_o\cdot\hat{e}_2)\ \hat{e}_2 + (\hat{p}_o\cdot\hat{n})\ \hat{n},$$

$$\hat{q} = (\hat{q}\cdot\hat{e}_1)\ \hat{e}_1 + (\hat{q}\cdot\hat{e}_2)\ \hat{e}_2 + (\hat{q}_o\cdot\hat{n})\ \hat{n}, \qquad \text{where}$$

$\hat{n}$ is the unit normal to the surface, $\hat{n}$ being given by $\vec{r}_s/a$ (62), and the definition of $\hat{p}_o$, $\hat{q}$ in (61), we secure

$$\langle|G(r_s)|^2\rangle = \frac{3}{8}\, p^4 \cos^4\beta/2.$$

The value of the expected value of σ is then

$$\langle\sigma\rangle = \pi a^2 \left|\frac{5\ e\lambda 2}{12\pi}\right|^2 \frac{3}{2}\ p^4 \cos^2\beta/2 \qquad (5\text{-}66)$$

Consequently, if n dipoles are present in every $\frac{\lambda}{2} \times \frac{\lambda}{2}$ rectangle,

$$\left\langle\frac{\sigma}{\pi a^2}\right\rangle = \frac{3}{2}\, p^4 \cos^2\beta/2 \left|\frac{5n}{3\pi}\right|^2 \qquad (5\text{-}67)$$

In order for any significant enhancement to occur, it is necessary that $n \geq 2$; If $n > 3$, mutual coupling between the dipoles will become significant, making (65) an unreliable estimate. If $n=2$, the mutual coupling can be avoided by placing two orthogonal dipoles in each $\frac{\lambda}{2} \times \frac{\lambda}{2}$ cell.

5.3.1 Analysis of surface waves on a wire mesh balloon.

It has been found that a wire mesh balloon whose mesh size and wire radius is much less than a wavelength exhibits a radar cross section return having a gain over a metal sphere of equal radius. Analysis has been performed on a square wire loop in order to explain this phenomena. One may call this type of analysis a "microscopic approach". In this memo an attempt is made at explaining the problem by considering the entire balloon surface as a collection of randomly distributed square wire meshes and then looking at the overall surface phenomena associated with it, or in other words, a "macroscopic approach".

Experimental evidence on flat, square wire meshes has indicated that a surface wave phenomena does seem to exist which is not related to wire loop behavior and leads one to consider the broad properties of the mesh as opposed to the individual "loop" phenomena. When this is done it is found that the wire mesh has two main contributors: a flat plate contributor and a traveling wave contributor, where the traveling wave is noticed at aspects near edge on and the flat plate is noticed broadside to the mesh. From this analysis an extension is made to the case of a large sphere made up of a collection of wire mesh patches. This type of analysis is conducted assuming a collection of average mesh patches randomly distributed over the sphere. The computed results indicate that a gain over a metal sphere can be expected and the gain is both frequency and wire length dependent.

5.3.2 Flat Plate Analysis

In order to determine the behavior of a wire mesh whose mesh size is small compared to a wavelength an experiment was conducted on a plane wire mesh. The mesh was six inches square and placed on a flat piece of styrafoam.

The results were then calibrated to a flat metal plate for comparison. The measurements were made at two frequencies, 3.35 Kmc and 5.42 Kmc; the results at both horizontal and vertical polarizations at 5.42 Kmc are shown in Figures 5.22 and 5.23, and the results at just horizontal polarization at 3.35 Kmc is shown in Figure 5.24. The interesting thing about the results is that at aspects near edge on for horizontal polarization an increase over a flat plate is apparent for the 5.42 Kmc case but not the 3.35 Kmc case. In addition, the oscillatory behavior is also different in that the peak widths are broader than one would normally expect from just a flat plate type return. This indicates that small flat plates give rise to surface wave phenomena similar to traveling waves. At vertical polarization the results for both the flat plate and the wire mesh are identical except for a slight loss due to energy transmitted through the mesh.

In order to explain these results we hypothesize a surface wave phenomena occurring with the expected large flat plate behavior. The obvious surface wave phenomena is the traveling wave since we can consider each wire (or groups of wires) as a traveling wave generator. Under this assumption the average or random phase cross section for a wire mesh would simply be,

$$\langle \sigma \rangle = \sigma_{F.P.} + \sigma_{T.W.} \tag{5-68}$$

where

$$\sigma_{F.P.} = \frac{4\pi L^4}{\lambda^2} \sin^2\theta \; \frac{\sin^2 (kL \cos\theta)}{(kL \cos\theta)^2}$$

$$\sigma_{T.W.} = \frac{\lambda^2 \lambda^2}{\pi Q^2} \left\{ \frac{\sin\theta}{1 - p\cos\theta} \sin\left[\frac{kL}{2p} (1 - p\cos\theta) \right] \right\}^4$$

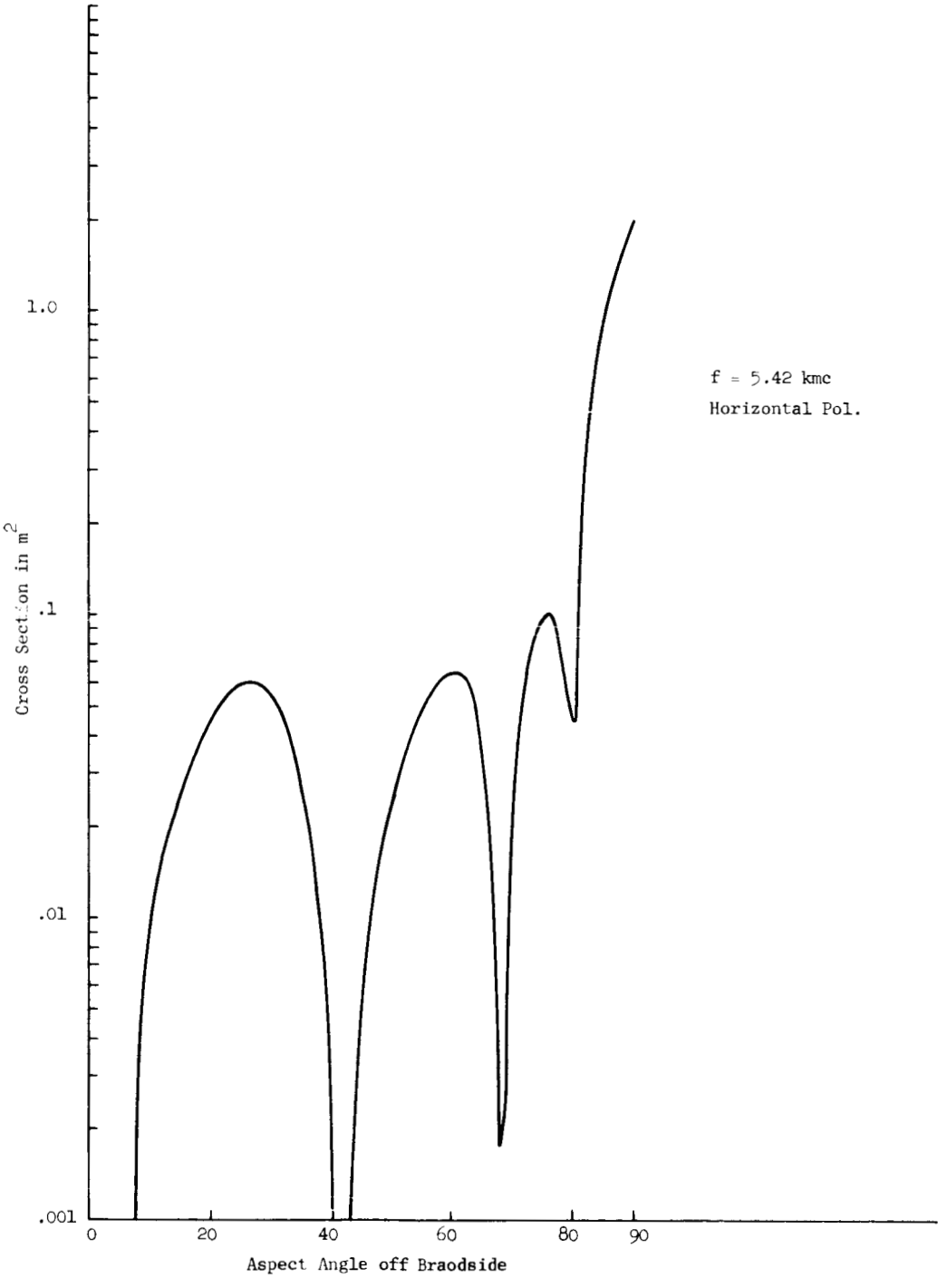

Figure 5.22 Cross Section of a 6" Wire Screen

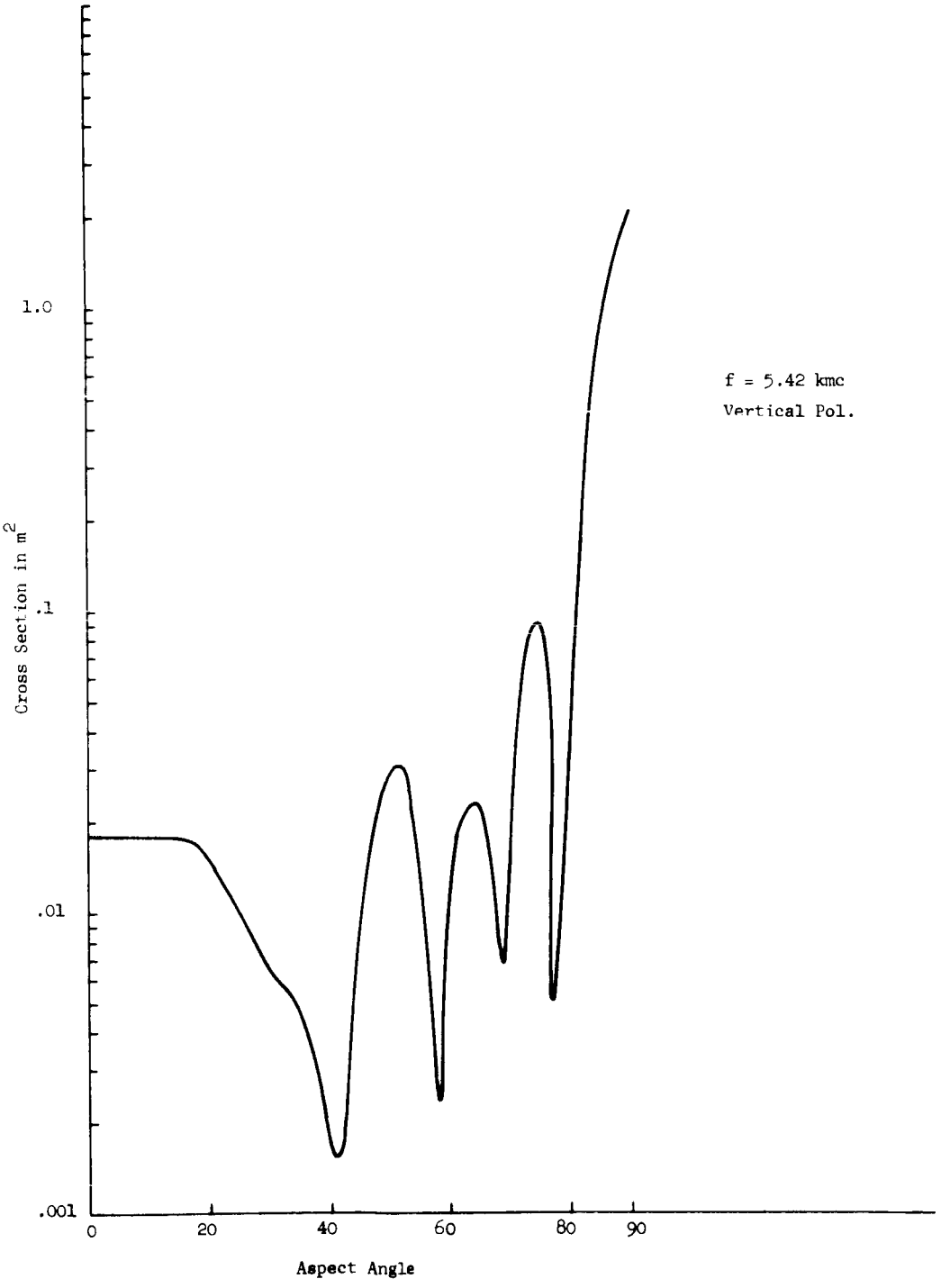

Figure 5.23 Cross Section of a 6" Wire Screen

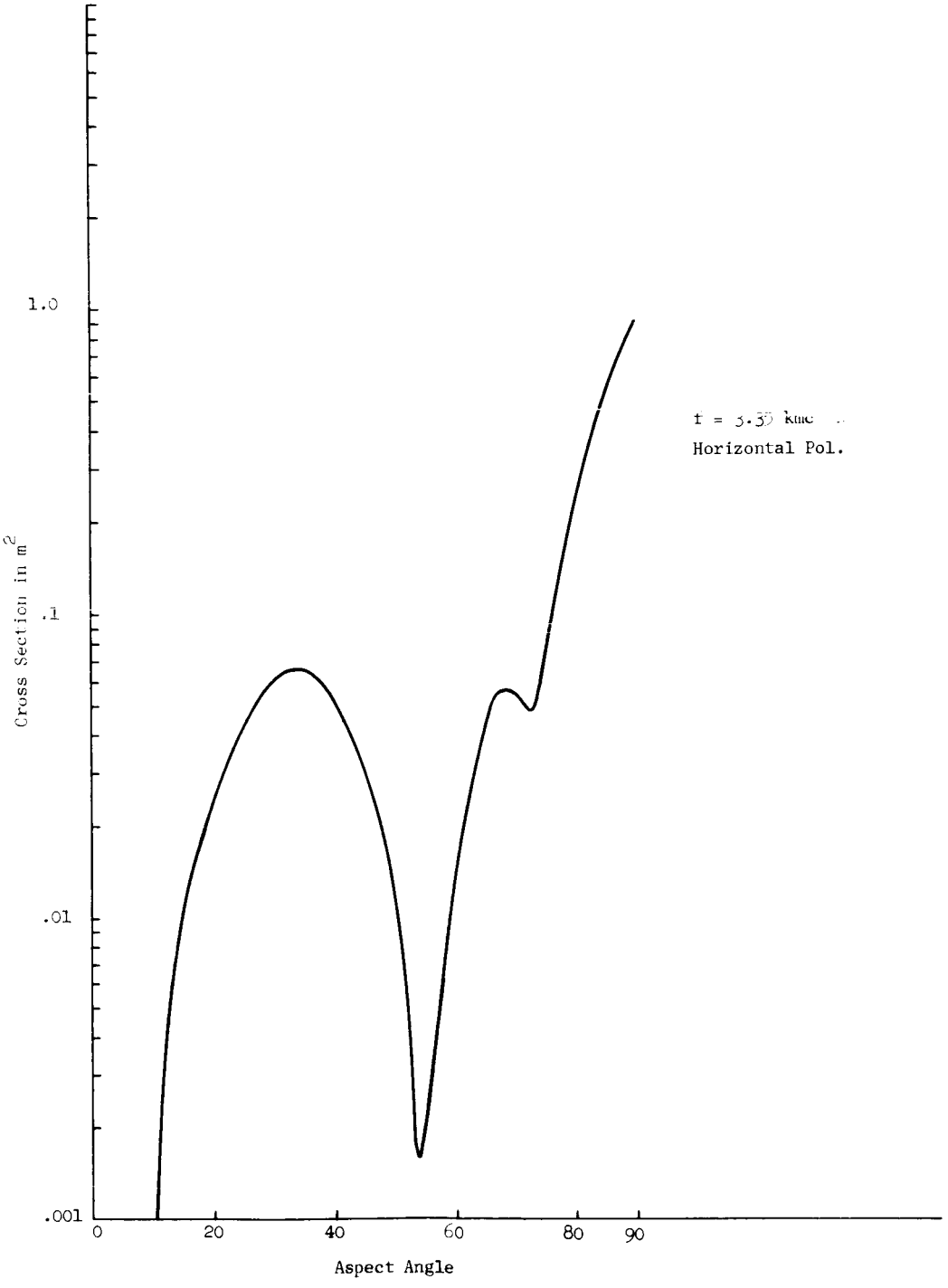

Figure 5.24 Cross Section of a 6" Wire Screen

and

$$Q = -\frac{2}{p^2} + \frac{C_{in}\left[\frac{kL}{p}(1+p)\right] - C_{in}\left[\left(\frac{kL}{p}\right)(1-p)\right]}{p^3} +$$

$$+ \frac{1}{2p^3}\left\{(p-1)\cos\left[\frac{kL}{p}(1+p)\right] + (p+1)\cos\left[\frac{kL}{p}(1-p)\right] + \right.$$

$$\left. + (p^2-1)\frac{kL}{p}\left[S_i\left[\frac{kL}{p}(1+p)\right] - S_i\left[\frac{kL}{p}(1-p)\right]\right]\right\}$$

p is the relative phase velocity

γ is the current reflection coefficient

L is the wire length.

In order to determine the validity of Equation (68) it is necessary to establish values for the relative phase velocity and the current reflection coefficient. The wire mesh is coated with a plastic material whose dielectric constant is greater than one. So we would expect a value for p less than one and it is found that $p \simeq .93$. The current reflection coefficient, γ, is a much more subtle quantity in that at present no analytical methods are available for determining its value. We would expect, however, that γ would be sensitive to both frequency and mesh size since the number of traveling wave generators would depend on both these quantities. By fitting the experimental results to the theoretical calculation we find that γ is about 2.1 and that γ increases slightly for increasing frequency.

The results obtained using the above information are shown in Figures 5.25 and 5.26. It is seen from these results that the cross section for the wire mesh is closely matched using random phase addition. The deviation from the experiment could no doubt be explained had we taken phase into account. We can therefore conclude that a traveling wave gives rise to the gain over a large flat plate at aspects near edge on for a horizontally polarized plane wave.

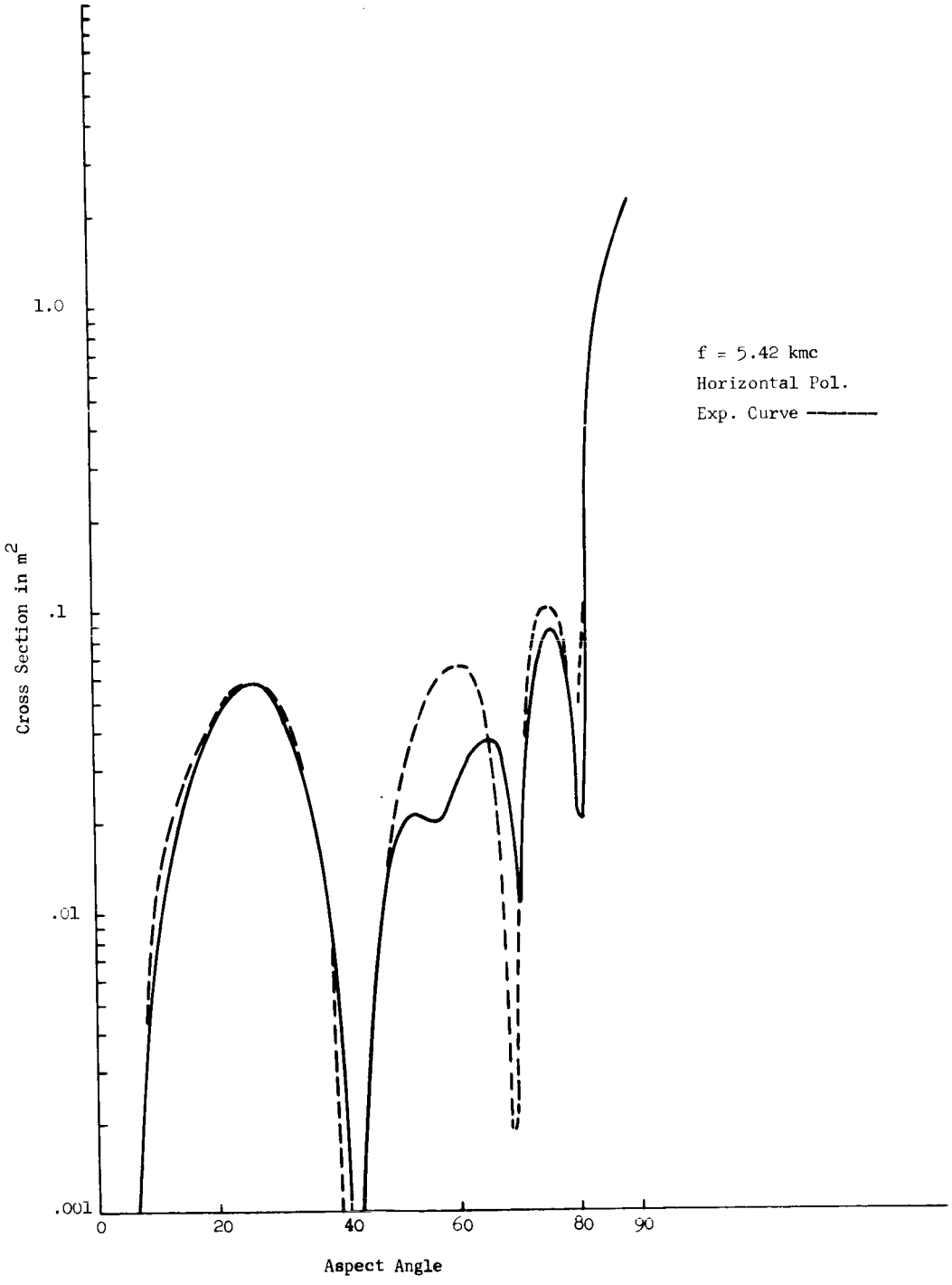

Figure 5.25 Theoretical Cross Section of a 6" Wire Mesh

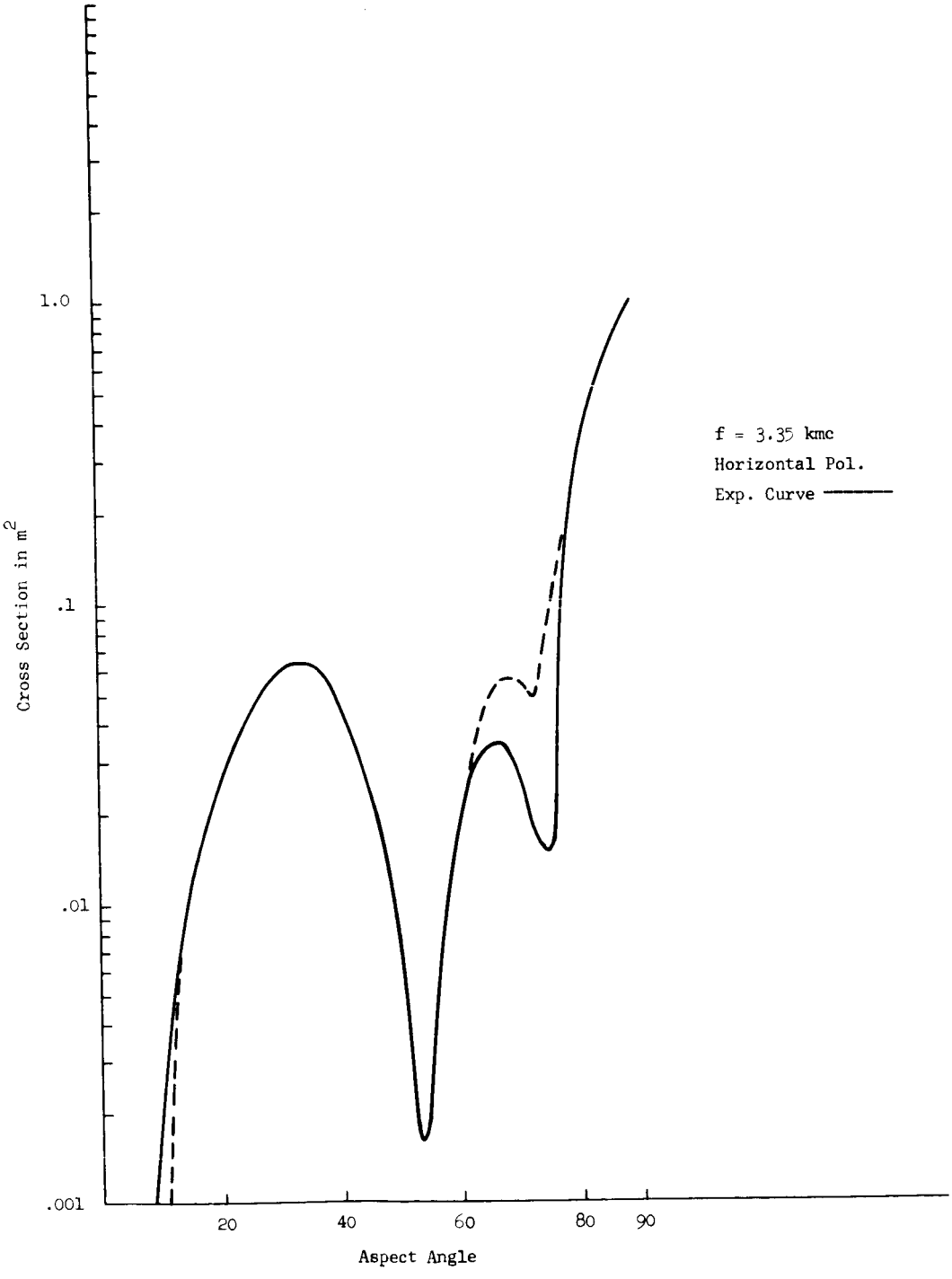

Figure 5.26 Theoretical Cross Section of a 6" Wire Mesh

5.4 Balloon Analysis

The purpose of the preceding section is to establish a theoretical approach in the hope of explaining the gain found over a metal sphere when the sphere is composed of wire meshes. The sphere in question consists of a collection of pentagonal and hexagonal wire mesh patches imbedded in a mylar film. The patch descriptions are shown in Figure 5.27. In order to obtain a meaningful analysis for such a sphere some kind of averaging process is necessary to extend the previous results to cover the case of a wire mesh sphere. Therefore, the following assumptions are made: The sphere can be thought of as a collection of square mesh patches randomly distributed over the surface; each patch has the same probability of being oriented along the incident polarization vector; the scattered field due to each patch can be added in a random phase fashion. These assumptions, which are not unreasonable owing to the size of the sphere and the number of patches, leads us then to the following analysis.

The patches are first analyzed to obtain an average wire length and an average number of wires per patch. We then compute a weighted average over the total number of patches used based on how many of each type of patch are on the sphere. This gives us a collection of square patches 27.3" on a side consisting of 220 wires per patch. The other assumptions now allow us to write the cross section of the wire mesh sphere as,

$$\sigma = \sigma_{\text{sphere}} \frac{+\int_0^{2\pi} \int_0^{\pi/2} \sigma_{T.W.} \cos^2\varphi \, d\varphi}{\int_0^{2\pi} d\varphi} \qquad (5\text{-}69)$$

where φ is the angle made by each patch with the polarization vector. Equation (69) when the appropriate values for σ_{sphere} and $\sigma_{T.W.}$ are inserted becomes,

$$\sigma = \pi r^2 + \frac{1}{2} \frac{\gamma^2 \gamma^2}{\pi Q^2} \left(\frac{kL}{2p} \right)^4 \int_0^{\pi/2} \sin^4\theta \, \frac{\sin^4\left[\frac{kL}{2p} (1-p\cos\theta) \right]}{\left[\frac{kL}{2p} (1-p\cos\theta) \right]^4} \, d\theta \qquad (5\text{-}70)$$

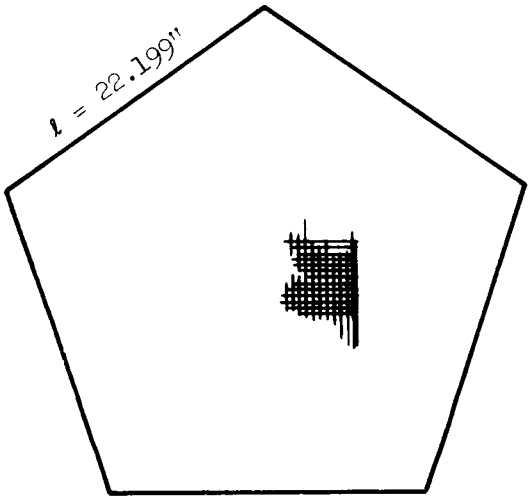

Type A 12 Each

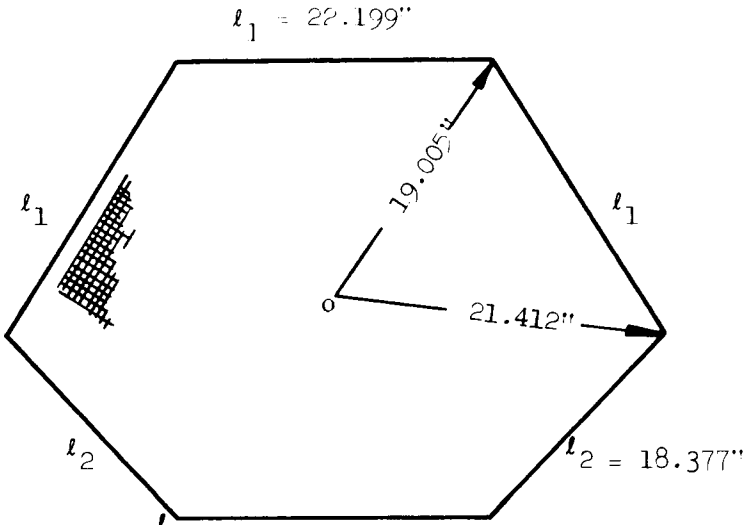

Type B 60 Each

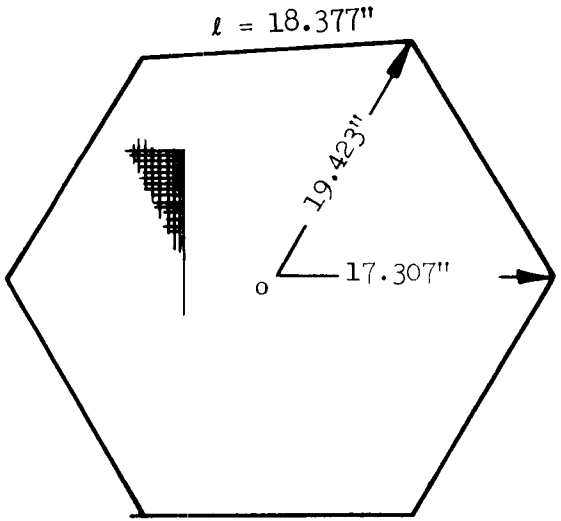

Type C 20 Each

Coating: 1/2 Mil C Mylar

Wire: 3 Mil Copper

Wire Separation: 0.169"

Figure 5.27 Wire Mesh Patches

or,

$$\sigma = \pi r^2 + \frac{1}{2} \quad \frac{\gamma^2 \lambda^2}{\pi Q^2} \left(\frac{kL}{2p} \right)^4 I$$

In order to evaluate the integral in Equation (70), we must introduce further approximations, namely $kL \gg 1$, $p < 1$ and that $\sin^3\theta$ does not vary greatly between $\theta = 0$ and $\theta = \cos^{-1}\sqrt{\frac{2}{3}}\, p$. This is certainly not unreasonable since most measurements will be between S and C band, and for the sphere p is less than 1 but greater than 0.9. When this is done we obtain,

$$I \simeq \frac{2}{kL} \left[\left(\frac{1}{3}\right)^{3/2} - 1 + \frac{3}{2p^2} \right] \left| \pi - \frac{\sin^3 \left[\frac{kL}{2p} \left(1 - \sqrt{\frac{2}{3}}\, p\right) \right]}{\left[\frac{kL}{2p} \left(1 - \sqrt{\frac{2}{3}}\, p\right) \right]^2} \right. \times$$

$$\times \left\{ \frac{\sin \left[\frac{kL}{2p} \left(1 - \sqrt{\frac{2}{3}}\, p\right) \right]}{\frac{kL}{2p} \left(1 - \sqrt{\frac{2}{3}}\, p\right)} + 2 \cos \left[\frac{kL}{2p} \left(1 - \sqrt{\frac{2}{3}}\, p\right) \right] \right\} \Bigg| +$$

$$+ \frac{2}{kL} \left(1 - \frac{3}{2p^2}\right) \left[\pi - \frac{\sin^3 \frac{kL}{2p}}{\left(\frac{kL}{2p}\right)^2} \left(\frac{\sin \frac{kL}{2p}}{\frac{kL}{2p}} + 2 \cos \frac{kL}{2p} \right) \right] +$$

$$+ \frac{12}{p(kL)^2} \left[\frac{\sin \frac{kL}{p}}{\frac{kL}{p}} - \frac{\sin \frac{2kL}{p}}{\frac{2Kl}{p}} - \frac{\sin^3 \frac{kL}{2p}}{\frac{kL}{2p}} \left(\frac{\sin \frac{kL}{2p}}{\frac{kL}{p}} + 2 \cos \frac{kL}{2p} \right) \right.$$

$$- \frac{\sin \frac{kL}{p} \left(1 - \sqrt{\frac{2}{3}}\, p\right)}{\frac{kL}{p} \left(1 - \sqrt{\frac{2}{3}}\, p\right)} + \frac{\sin \frac{2kL}{p} \left(1 - \sqrt{\frac{2}{3}}\, p\right)}{\frac{2kL}{p} \left(1 - \sqrt{\frac{2}{3}}\, p\right)} +$$

$$\left. + \frac{\sin^3 \left[\frac{kL}{2p} \left(1 - \sqrt{\frac{2}{3}}\, p\right) \right]}{\frac{kL}{2p} \left)1 - \sqrt{\frac{2}{3}}\, p\right)} \left\{ \frac{\sin \frac{kL}{2p} \left(1 - \sqrt{\frac{2}{3}}\, p\right)}{\frac{kL}{p} \left(1 - \sqrt{\frac{2}{3}}\, p\right)} + 2 \cos \frac{kL}{2p} \left(1 - \sqrt{\frac{2}{3}}\, p\right) \right\} \right] -$$

$$- \frac{9}{(kL)^3} \left[\frac{-p}{kL} + \frac{p}{kL \left(1 - \sqrt{\frac{2}{3}}\, p\right)} \right]$$

Since kL >> 1 we can express the above in terms of a series involving powers of 1/kL so that to order $(1/kL)^2$ we can write

$$I \simeq \frac{\lambda}{L} \left(\frac{1}{3}\right)^{3/2} + O\left(\frac{1}{k^2L^2}\right) \qquad (5\text{-}71)$$

This gives for the cross section of the balloon,

$$\sigma \simeq \pi r^2 + \frac{\gamma^2 \pi^3}{2(3)^{3/2} p^4} \frac{L^3}{\lambda Q^2} \qquad (5\text{-}72)$$

We must still determine γ and p for the wire mesh patches. If the wire is imbedded in a material whose dielectric constant is greater than one, then p will be some number less than one, call it η, where for the flat mesh used before $\eta \simeq .93$. Since there will be a curvature associated with each patch on the sphere then p can be expressed as

$$p = \left\{ 1 - \frac{1}{12} \left(\frac{L}{r}\right)^2 \right\} \eta \ , \ \frac{L}{r} < 1 \qquad (5\text{-}73)$$

For a sphere of radius 84" and assuming η is again 0.93, $p \simeq 0.92$. It still remains to find a reasonable γ for the wire meshes used on the sphere. γ will also be effected by the curvature in addition to frequency and mesh size. However, based upon the flat mesh results we have determined a probable γ for the frequencies considered. We have then multiplied this γ by a factor of 0.7 since this seems to be about the value found for γ using curved bodies. Ref. 11. Further experimentation is necessary to determine a more accurate value of γ.

5.5 Conclusion

Since no further experimental results on the mesh sphere are available at this time no clear cut conclusions can be drawn. However, the results obtained do predict a gain over a metal sphere of the order of magnitude found by past experiments using a similar balloon at the high frequency. Figure 5.28

---

11 End-Fire Echo Area of Long, Thin Bodies, L. Peters, PCAP, 1/58, Pgs. 132-139

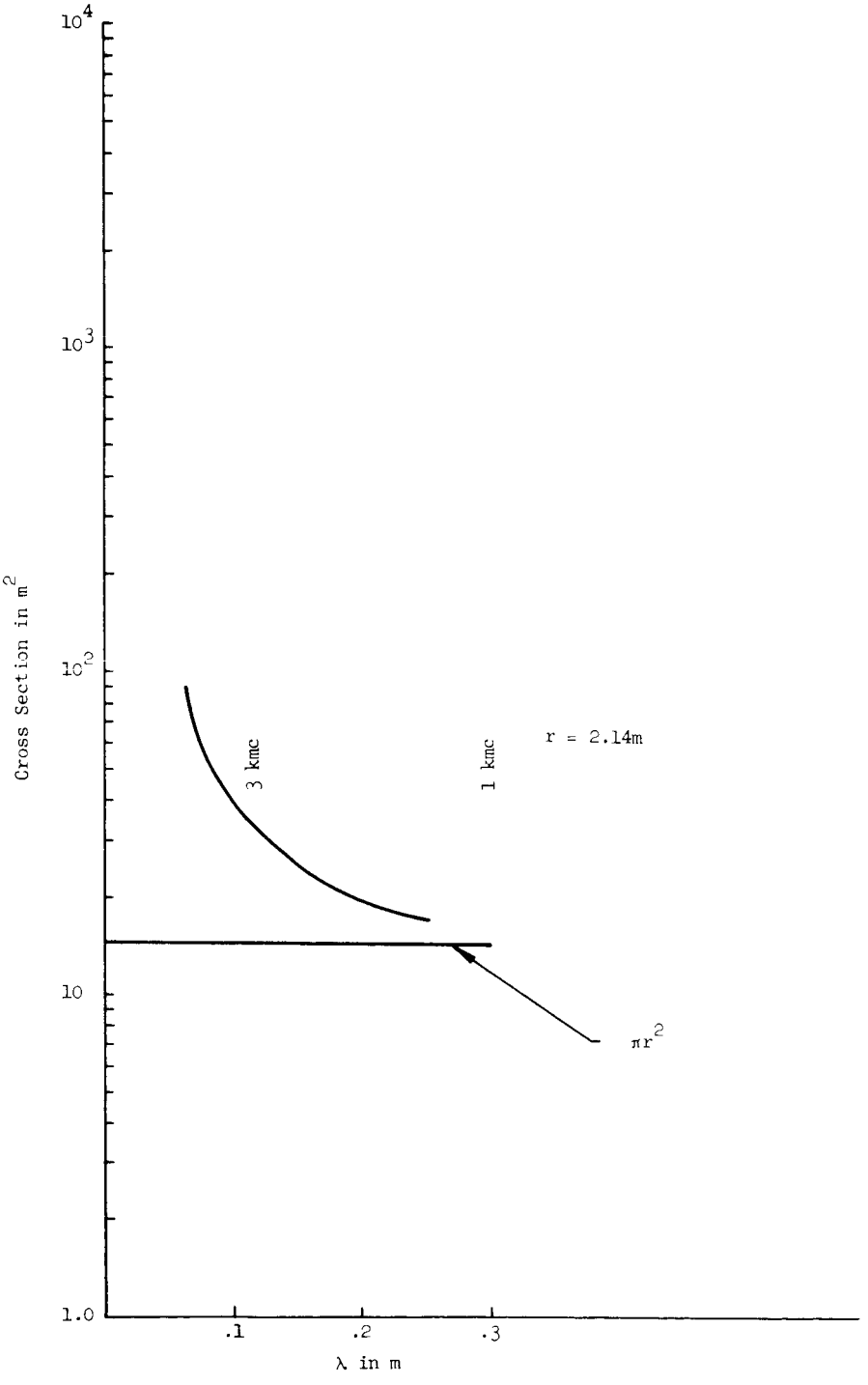

Figure 5.28 Cross Section Vs. λ for a Wire Mesh Sphere

shows the expected results down to L band where surprisingly the additional contribution of a traveling wave is found to be less than at C band. Since this is a first order approach to the problem we cannot expect remarkably accurate results, however, if further experimentation indicates that this is the proper approach additional analysis on a more exact basis should be carried out.

Another important result is that small flat plates give rise to noticeable surface waves which originate at the edge of the plate and behave in similar fashion to a traveling wave. Since the coating on the mesh was an important consideration in determining the results one would expect that a coated small flat plate would accomplish about the same results. This hypothesis is certainly worth looking into.

In the preceding, a theory had been worked out whereby it was postulated that one would expect a traveling wave phenomenon along with the physical optics results when observing the radar cross section of a flat wire mesh patch. The traveling wave cross section associated with a wire was used to determine the additional contribution. The theory is now extended and the traveling wave cross section for a flat wire mesh is determined from antenna theory. The results are then computed and compared to the previous experimental results. It is shown that excellent agreement both qualitatively and quantitatively are obtained. We again extend the results to consider what one would expect when observing a balloon entirely made up of wire mesh patches. However, instead of integrating the traveling wave over the entire sphere we merely sum the major contribution. This leads to results very similar to those previously obtained. The major difference is that now, γ, the voltage (or current) reflection coefficient is a more meaningful entity since it is entirely dependent upon the patch itself and not on the single wire concept as before. We still are left with the dilemma of determining γ for the patch; however, this can be done experimentally on either flat or curved patches. Preliminary results do indicate that γ is proportional to sin as other experiments (12) have indicated. It is also noted that γ will vary with wavelength and in all likelihood it will vary with plate termination and relative phase velocity, p. How these other factors will effect γ can only be guessed at but further experiments may lead to more exact determination.

In order to compute the radar cross section of a flat plate which takes into account the traveling wave we will derive an expression similar to Peter's (13) expression for long, thin bodies. The radar cross section due to the traveling wave on an antenna is given by

$$\sigma_{t.w.} = \frac{\gamma^2 \lambda^2}{4\pi} G^2(\theta,\varphi) \qquad (5\text{-}74)$$

where $G(\theta,\varphi)$ is the gain function of the antenna at some point other than maximum. The gain function can be expressed as (14);

Reference 12: E. LeBaron, Conductron Memo D6610-9-M, June 1962
Reference 13: L. Peters, End-Fire Echo Area of Long, Thin Bodies, PGAP, P.133 - 139, Jan. 1958
Reference 14: J. D. Krauss, Antennas, McGraw-Hill Book Co. Inc., N.Y., N.Y. p.27, 1950

$$G(\theta,\varphi) = G\,\frac{U}{U_m}$$

where U is the radiation intensity in the direction (θ,φ), U_m is the maximum radiation intensity and G is the gain. If we further assume that the antenna is lossless then

$$G(\theta,\varphi) = D\,\frac{f(\theta,\varphi)}{f(\theta,\varphi)_{max.}} \tag{5-75}$$

where D is the directivity and $f(\theta,\varphi)$ is the antenna pattern factor. Substituting (5-75) for $G(\theta,\varphi)$ into Equation (5-74) for σ gives

$$\sigma_{t.w.} = \frac{\gamma^2\lambda^2}{4\pi}\,D^2\,\frac{f^2(\theta,\varphi)}{f^2(\theta,\varphi)_{max.}} \tag{5-76}$$

Krauss (15) has shown that for a broadside rectangular array the directivity is given by

$$D = \frac{4\pi A}{\lambda^2}$$

where A is area of the array. He further stated that this directivity is valid even if the array is not necessarily rectangular. The pattern factor, $f(\theta,\varphi)$ is determined by the pattern factor for an individual wire which is oriented parallel to the electric field. If we assume $f(\theta,\varphi)$ is the same as one would find for a wire giving rise to a traveling wave, then for $\varphi = 0$,

$$\sigma_{t.w.} = \frac{4\pi A^2\gamma^2\sin^4\theta}{\lambda^2 f^2(\theta)_{max}}\left\{\frac{\sin^4[\frac{ka}{2p}\,(1-p\,\cos\,\theta)]}{(1-p\,\cos\theta)^4}\right\} \tag{5-77}$$

where a is the wire length and p the relative phase velocity.

Equation (5-77) then is the expected return due to traveling wave phenomena

---

Reference 15: J. D. Krauss, Antennas, McGraw-Hill Book Co. Inc., N.Y., N.Y. P.121, 1950

associated with a flat plate. In order to determine the cross section one observes from a flat plate we must also consider the well known optics return which is given by

$$\sigma_{f.p.} = \frac{4\pi A^2}{\lambda^2} \sin^2\theta \quad \frac{\sin^2(ka\cos\theta)}{(ka\cos\theta)^2} \tag{5-78}$$

By adding in random phase this leads to

$$= \frac{4\pi A^2}{\lambda^2} \quad \frac{\gamma^2 \sin^4\theta \sin^4 \quad \frac{ka}{2p}(1-p\cos\theta)}{f^2(\theta)_{max}\,(1-p\cos\theta)^4} + \frac{\sin^2\theta \sin^2(ka\cos\theta)}{(ka\cos\theta)^2} \tag{5-79}$$

Equation (5-79) was compared to the results obtained experimentally and it was found that γ could be written as $\gamma = \gamma_o \sin\theta$ where γ_o was about 0.28 but appeared to vary with wavelength. Since our results are for λ = .056m and λ = .085m this is certainly not conclusive. The results of experiment versus theory are shown in Figures 5.22, 23 . It is further noted that these results are for p = .92 which is about the same as previously indicated.

In order to extend our results to the balloon we again employ an averaging process of the patches and assume they are all rectangular and evenly distributed over the sphere. If we further assume a random distribution of wire orientation then we can write the average cross section due to the traveling wave over arbitrary linear polarization as

$$\overline{\sigma_{t.w.}} = \frac{1}{2\pi} \int_0^{2\pi} \sigma_{t.w.} \cos^4\varphi d\varphi = \frac{3}{8} \sigma_{t.w.} \tag{5-80}$$

At this point, instead of integrating over the sphere we must take into account that there are a finite number of patches on the illuminated side.

If we assume that it will only be necessary to consider those patches which give rise to the largest return then all we need do is sum over a band of average rectangular patches whose normal makes the angle with the incident vector that gives rise to the largest return. The sum of the traveling wave contributions due to these patches would then be

$$(\tfrac{3}{8})\ [\ \frac{2\pi r\ \cos(\theta max)}{a}\ ]\ \frac{4\pi A^2}{\lambda^2}\ \gamma_o^{\ 2}\ \sin^2(\theta max) \qquad (5\text{-}81)$$

where r is the sphere radius. In order to determine the cross section of the sphere we must add the specular return, however, since the panels will now have a curvature associated with them it would be unrealistic to add the flat plate return. Hence, as before, we add in random phase the specular return from the sphere and this gives,

$$<\sigma> = \pi r^2 + \frac{3\pi^2 r a^3}{\lambda^2}\ \gamma_o^2\ \cos\ (\theta max)\ \sin^2(\theta max) \qquad (5\text{-}82)$$

If in addition ka is large we can approximate θ_{max} by

$$\theta_{max} \quad \frac{\lambda}{a}\ (0.861)\ \text{radians}$$

so that,

$$\sin^2(\theta_{max}) \quad (0.861)^2\ \ \frac{\lambda}{a}$$

Then our expression for $<\sigma>$ becomes

$$<\sigma> \ \_\ \pi r^2 + \frac{22 r a^2}{\lambda}\ \ \gamma_o^2 \qquad (5\text{-}83)$$

Figure 5.29 is a plot of Equation (5-83) over a small range of λ primarily because we chose $\gamma_o = .28$ which is what was obtained for flat plate data near these frequencies. Since we would expect γ_o to vary with frequency, terminations and coatings, further extensions of Equation (5-83) without more

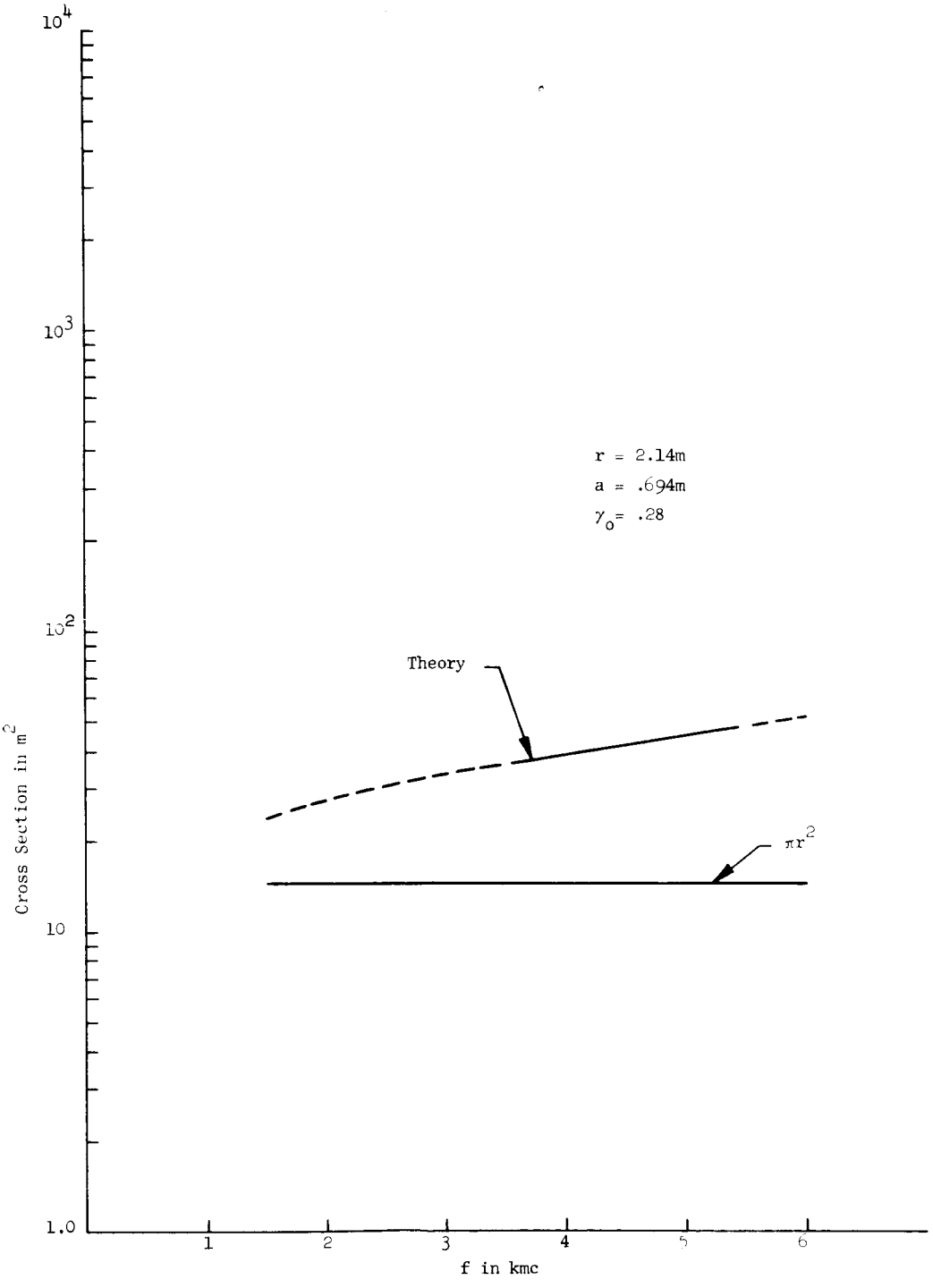

Figure 5.29 Cross Section of a Wire Mesh Balloon

substantial information on γ_o is unreasonable.

The results, as before, indicate a gain over the sphere on the average. We must also take into account that in reality one would expect a rapid oscillatory behavior as a function of aspect since there will be many phase effects from all the contributors. We would not expect large oscillations since due to the multiplicity of contributors only a very few would be either in or out of phase whereas most would be randomly phased. The task of computing the fine structure would be formidable especially at the frequencies of interest. It is therefore felt that the random phase approach is the most reasonable approach to this problem.